Experimental Characterization of Models for Backbone Picosecond Dynamics in Proteins. Quantification of NMR Auto- and Cross-correlation Relaxation Mechanisms Involving Different Nuclei of the Peptide Plane

Mark W. F. Fischer,[†,‡] Lei Zeng,[†,||] Yuxi Pang,[†] Weidong Hu,[†,#] Ananya Majumdar,[†,#,○] and Erik R. P. Zuiderweg*[,†,§,⊥]

Contribution from the Biophysics Research Division, Department of Physics, Department of Biological Chemistry, and Department of Chemistry, The University of Michigan, 930 North University Avenue, Ann Arbor, Michigan 48109

Received June 24, 1997. Revised Manuscript Received September 9, 1997[⊗]

Abstract: NMR relaxation parameters were measured for the peptide-plane carbonyl and nitrogen nuclei for the protein *Escherichia coli* flavodoxin. A poor correlation between the general order parameters of the C′−Cα vector (Zeng, L.; Fischer, M. W. F.; Zuiderweg, E. R. P. *J. Biomol. NMR* **1996**, *7*, 157−162) and the N−NH vector was observed. We interpret this lack of correlation in this nearly spherical protein as evidence of local or semilocal anisotropic motion. A new experiment is introduced from which the cross-correlation between the carbonyl chemical shift anisotropy relaxation and carbonyl-Cα dipole−dipole relaxation is obtained. We show theoretically that the three relaxation measurements, reporting on the dynamics of the C′−Cα vector, N−NH vector, and CSA tensor components behave differently under anisotropic motion. The cross-correlation order parameter formalism for dipolar cross-correlation spectral densities, as introduced by Daragan and Mayo (Daragan, V. A.; Mayo, K. H. *J. Magn. Reson. B* **1995**, *107*, 274−278), has been extended to include cross-correlations between nonaxial chemical shift anisotropy and dipole−dipole relaxation. By analyzing our experimental data with the theoretical models for anisotropic local motion, dynamic models were obtained for the peptide planes of 32 residues of *E. coli* flavodoxin.

The understanding of protein function is incomplete without considering dynamics.[1] Large scale and probably slow dynamics, mostly inferred from static measurements, is in some cases thought to be essential to protein function, e.g., the opening of the myoglobin heme pocket to allow access of oxygen,[2] flap movements in enzymes to sequester substrates,[3] and conformational changes in signal transduction factors to transmit information.[4] Smaller scale dynamics, i.e., the motion of individual protein backbone and side-chain atoms, is known to occur from direct evidence such as crystallographic B-factors, from computational simulation of molecular dynamics, and from the measurement of backbone dynamics from amide nitrogen NMR relaxation. The extent of these motions is known reasonably well (B-factors, NMR order parameters, and MD trajectories). Their frequencies can be obtained experimentally from NMR data and are found to be on the picosecond timescale.[5] Functions for these fast local motions are not so easy to envision. Potentially, small-scale local motions could allow active-site residues in enzymes to make transient contact with the substrate to effect the enzyme's chemistry without requiring exceedingly precise geometry. Picosecond dynamics is certainly associated with retention of entropy in the folded state. Attempts are being made to relate changes in NMR order parameters upon ligand binding to changes in protein entropy.[6] Recently, measurements of the change in picosecond dynamics upon protein−ligand interaction were used to obtain a footprint of the interaction site.[7] As picosecond protein dynamics could be of relevance to the retention of entropy of the bound ligand,[8] these footprints may however go undiscovered, especially when one only observes the reorientational dynamics of a single internuclear axis.

* To whom correspondence should be addressed at zuiderwe@umich.edu.
† Biophysics Research Division.
‡ Department of Physics.
§ Department of Biological Chemistry.
⊥ Department of Chemistry.
|| Present address: Mount Sinai Hospitals, New York.
Present address: Sloan-Kettering Cancer Center, New York.
○ On leave from the Tata Institute of Fundamental Research, Mumbai 40005, India.
⊗ Abstract published in *Advance ACS Abstracts*, December 1, 1997.

(1) Wagner, G. *Nature Struct. Biol.* **1995**, *2*, 255−256. Palmer, A. G. *Curr. Opin. Biotechnol.* **1993,** *4*, 385−91. Dayie, K. T.; Wagner, G.; Lefevre, J. F. *Annu. Rev. Phys. Chem.* **1996**, *47*, 243−82. Nicholson, L. K.; Yamazaki, T.; Torchia, D. A.; Grzesiek, S.; Bax, A.; Stahl, S. J.; Kaufman, J. D.; Wingfield, P. T.; Lam, P. Y.; Jadhav, P. K.; Hodge, C. N.; Domaille, P. J.; Chang, C. H. *Nature Struct. Biol.* **1995**, *2*, 274−80. Mandel, A. M.; Akke, M.; Palmer, A. G., III. *J. Mol. Biol.* **1995**, *246*, 144−163.

(2) Karplus, M.; Petsko, G. A. *Nature* **1990**, *347*, 631−639.

(3) Nicholson, L. K.; Yamazaki, T.; Torchia, D. A.; Grzesiek, S.; Bax, A.; Stahl, S. J.; Kaufman, J. D.; Wingfield, P. T.; Lam, P. Y.; Jadhav, P. K.; Hodge, C. N.; Domaille, P. J.; Chang, C. H. *Nature Struct. Biol.* **1995**, *2*, 274−80. Cox, S.; Radzio-Andzelm, E.; Taylor, S. S. *Curr. Opin. Struct. Biol.* **1994**, *4*, 893−901. Farber, H. R.; Matthews, B. W. *Nature* **1990**, *384*, 263−266.

(4) Milburn, M. V.; Tong, L.; DeVos, A. M.; Brünger, A.; Yamaizumi, Z.; Nishimura, S; Kim, S.-H. *Science* **1990**, *247*, 939−945. Zu, Y. L.; Ai, Y.; Gilchrist, A.; Labadia, M. E.; Sha'afi, R. I.; Huang, C. K. *Blood* **1996**, *87*, 5287−5296. Hohenegger, M.; Nanoff, C.; Ahorn, H.; Freissmuth, M. *J. Biol. Chem.* **1994**, *269*, 32008−32015.

(5) Kay, L. E.; Torchia, D. A.; Bax, A. *Biochemistry* **1989**, *28*, 8972−8979. Clore, G. M.; Driscoll, P. C.; Wingfield, P. T.; Gronenborn, A. M. *Biochemistry* **1990**, *29*, 7387−7401. Clore, G. M.; Szabo, A.; Bax, A.; Kay, L. E.; Driscoll, P. C.; Gronenborn, A. M. *J. Am. Chem. Soc.* **1991**, *112*, 4989−4991. Barbato, G.; Ikura, M.; Kay, L. E.; Pastor, R. W.; Bax, A. *Biochemistry* **1992**, *31*, 5269−5278. Peng, J. W.; Wagner, G. Methods Enzymol. **1994**, 239, 563−96; Buck, M.; Boyd, J.; Redfield, C.; MacKenzie, D. A.; Jeenes, D. J.; Archer, D. B.; Dobson, C. M. *Biochemistry* **1995**, *34*, 4041−4055.

(6) Akke, M.; Brüschweiler, R.; Palmer, A. G, III. *J. Am. Chem. Soc.* **1993**, *115*, 9832−9833. Kay, L. E.; Muhandiram, D. R.; Farrow, N. A.; Aubin, Y.; Forman-Kay, J. D. *Biochemistry* **1996**, *35*, 361−368. Mandel, A. M.; Akke, M.; Palmer, A. G. *J. Mol. Biol.* **1995**, *246*, 144−63. Yang, D.; Kay, L. E. *J. Mol. Biol.* **1996**, *263*, 369−382.

S0002-7863(97)02083-0 CCC: $14.00

NMR relaxation measurements that determine protein dynamical parameters have generally focused on nearly ideal two-spin systems such as ^{15}N−NH, where the ^{15}N nucleus is relaxed through chemical shift anisotropy (CSA) and dipole−dipole interaction with the attached amide proton,[9] or the relaxation of natural abundance ^{13}Cα, dominated by the dipolar interaction with the attached proton.[10] In such cases, the relaxation of the heteronucleus can be ascribed to the reorientation of the HX internuclear vector with respect to the magnetic field direction. The strength of the use of (approximate) two-spin systems is that the relaxation data can be interpreted in terms of the local motion of the magnetic interaction vector superimposed on overall molecular tumbling.[11] The amount of local motion is often expressed with a generalized order parameter and, when the data are of sufficient sensitivity, correlation times characterizing the time scales of the local motions can be obtained.[12] Sometimes even faster local motions with their own order parameters and correlation times, superimposed on both previous motions, have been reported.[13] The method of spectral density mapping at five[14] or three[15] frequencies also focuses on obtaining the dynamics of single HX internuclear vectors.

As powerful as these methods focusing on the relaxation properties of a single internuclear vector may be in identifying areas of motion, they are deficient in that no description of the local motion is given. Only in the case when it can be assumed that the local motions of an internuclear vector is azimuthally symmetrical about an axis, can the generalized order parameter be interpreted as a special order parameter with $S^2 = {}^1/_2(3\cos^2\theta - 1)$, where θ is the angle between the vector and the symmetry axis.[11] Since it is difficult to prove that such a motion exists, it is generally deemed safest to not model the motion at all. This is of course an undesirable situation, which renders NMR picosecond dynamics measurements less informative than they might be.

Here we describe an approach that aims to obtain motional models for protein peptide planes. Motional models for picosecond dynamics are important for the better understanding of protein dynamics and can be used to help calibrate theoretical forcefields for computer simulation of dynamics.[16] They will help distinguish between random movements and correlated motions which is of great value for understanding protein function[17] and will help assess the degrees of freedom associated with entropy, and which degrees of freedom are retained upon ligand binding.[7] Motional models may ultimately be of help in the understanding of the activation barriers associated with conformational changes.[18] We concentrate on the measurement of the relaxation of a more complicated spin system, the C′ resonance of the polypeptide backbone, in a fully labeled and protonated protein. Figure 1 gives the definition of the C′ chemical shift tensor axes. Magnitudes of the different relaxation rates associated with the different magnetic interactions are listed in Table 1. The table shows that many interactions are significant for C′ relaxation. Several studies of C′ relaxation in proteins have recently appeared. In the work of Dayie and Wagner,[19] Allard and Härd,[20] and that of Engelke and Rüterjans,[20] C′ relaxation was measured from T_1 and T_2 data. In our previous work,[21] as well as that of Cordier et al.,[22] we study the Cα→C′ NOE which isolates the dipolar C′−Cα relaxation mechanism from all the other mechanisms. Our approach here is to continue to design different experiments to isolate and measure (pairs of) relaxation mechanisms, compare the efficiencies of the different mechanisms and combine this information to develop models for the local motion. For example, a local motion that can be described as a rotation about the C′−N bond vector or an axis parallel to the C′−N bond vector, will not engage the C′−N dipolar relaxation, since the C′−N vector is not reoriented, but will modulate the orientation of the C′−Cα vector with respect to the external magnetic field, thus causing relaxation due to the latter interaction. The anisotropic motion can be local, concerted for several residues (semilocal dynamics), or pertain to the entire molecule. Here we demonstrate differential relaxation effects by measuring the C′−Cα dipolar (auto-correlation) relaxation, the C′(CSA)/C′−Cα(dipolar) cross-correlation relaxation and conventional N−NH relaxation. With those, we can distinguish between several motional models for the individual peptide planes. We also show that a particular relaxation parameter, e.g., the N−NH relaxation order parameter, can fail to report local dynamics, while the other two measurements demonstrate its presence. We demonstrate our approach in detail by characterizing the back bone motions of

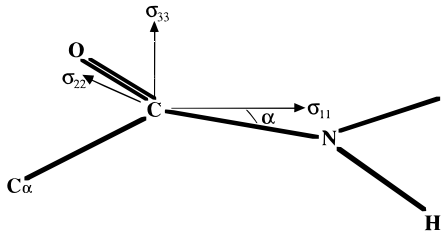

Figure 1. Orientations of the principal axes of the average carbonyl chemical shift tensor as defined in Table 2.

(7) Cheng, J. W.; Lepre, C. A.; Moore, J. M. *Biochemistry* **1994**, *33*, 4093−4100. Farrow, N. A.; Muhandiram, R.; Singer, A. U.; Pascal, S. M.; Kay, C. M.; Gish, G.; Shoelson, S. E.; Pawson, T.; Forman-Kay, J. D.; Kay, L. E. *Biochemistry* **1994**, *33*, 5984−6003. Hoyt, D. W.; Harkins, R. N.; Debanne, M. T.; O'Connor-McCourt, M.; Sykes, B. D. *Biochemistry* **1994**, *33*, 15283−15292. Stivers, J. T.; Abeygunawardana, C.; Mildvan, A. S. *Biochemistry* **1996**, *35*, 16036−16047.

(8) Yu, L.; Zhu, C. X.; Tse-Dinh,Y. C.; Fesik, S. W. *Biochemistry* **1996**, *35*, 9661−9666. Kay, L. E.; Muhandiram, D. R.; Farrow, N. A.; Aubin, Y.; Forman-Kay, J. D. *Biochemistry* **1996**, *35*, 361−368.

(9) Nirmala, N. R.; Wagner, G. *J. Am. Chem. Soc.* **1988**, *113*, 7557−7558. Kay, L. E.; Torchia, D. A.; Bax, A. *Biochemistry* **1989**, *28*, 8972−8979.

(10) Mispelter, J.; Lefevre, C.; Adjadj, E.; Quiniou, E.; Favaudon, V. *J. Biomol. NMR* **1995**, *5*, 233−244. Allard, P.; Jarvet, J.; Ehrenberg, A.; Graslund, A. *J. Biomol. NMR* **1995**, *5*, 133−146. Wand, A. J.; Urbauer, J. L.; McEvoy, R. P.; Bieber, R. J. *Biochemistry* **1996**, *35*, 6116−6125. Kay, L. E.; Bull, T. E.; Nicholson, L. K.; Griesinger, C.; Schwalbe, H.; Bax, A.; Torchia, D. A. *J. Magn. Reson.* **1992**, *100*, 538−558. Kushlan, D. M.; LeMaster, D. M. *J. Am. Chem. Soc.* **1993**, *115*, 11026−11027. Palmer, A. G., III; Hochstrasser, R. A.; Millar, D. P.; Rance, M.; Wright, P. E. *J. Am. Chem. Soc.* **1993**, *115*, 6333−6336. Nicholson, L. K.; Kay, L. E.; Baldisseri, D. M.; Arango, J.; Young, P. E.; Bax, A.; Torchia, D. A. *Biochemistry* **1992**, *31*, 5253−5263. Yamazaki, T.; Muhandiram, R.; Kay, L. E. *J. Am. Chem. Soc.* **1994**, *116*, 8266−8278. Engelke, J; Rüterjans, H. *J. Biomol. NMR* **1995**, *5*, 173−182.

(11) Lipari, G.; Szabo, A. *J. Am. Chem. Soc.* **1982**, *104*, 4546−4559. Lipari, G.; Szabo, A. *J. Am. Chem. Soc.* **1982**, *104*, 4559−4570.

(12) Clore, G. M.; Driscoll, P. C.; Wingfield, P. T.; Gronenborn, A. M. *Biochemistry* **1990**, *29*, 7387−7401.

(13) Clore, G. M.; Szabo, A.; Bax, A.; Kay, L. E.; Driscoll, P. C.; Gronenborn, A. M. *J. Am. Chem. Soc.* **1991**, *112*, 4989−4991.

(14) Peng, J. W.; Wagner, G. *Biochemistry* **1992**, *31*, 8571−8586. Peng, J. W.; Wagner, G. *Biochemistry* **1995**, *34*, 16733−16752. Peng, J. W.; Wagner, G. *J. Magn. Reson.* **1992**, *98*, 308−332.

(15) Farrow, N. A.; Zhang, O.; Szabo, A.; Torchia, D. A.; Kay, L. E. *J. Biomol. NMR* **1995**, *6*, 153−162. Ishima, R.; Nagayama, K. *Biochemistry* **1995**, *34*, 3162−3171.

(16) Yamasaki, K.; Saito, M.; Oobatake, M.; Kanaya, S. *Biochemistry* **1995**, *34*, 6587−6601. Eriksson, M. A.; Berglund, H.; Hard, T.; Nilsson, L. *Proteins* **1993**, *17*, 375−390. Zheng, Z.; Czaplicki, J.; Jardetzky, O. *Biochemistry* **1995**, *34*, 5212−5223. Tolman, J. R.; Flanagan, J. M.; Kennedy, M. A.; Prestegard, J. H. *Nature Struct. Biol.* **1997**, *4*, 292−297.

(17) Amadei, A.; Linssen, A. B. M.; Berendsen, H. J. C. *Proteins* **1993**, *17*, 412−425. Ikura, T.; Gō, N. *Proteins* **1993**, *16*, 423−436.

(18) Frauenfelder, H.; Parak, F.; Young, R. D. *Annu. Rev. Biophys. Biophys. Chem.* **1988**, *17*, 451−479.

(19) Dayie, K. T.; Wagner, G. *J. Magn. Reson. B* **1995**, *109*, 105−108.

(20) Allard, P.; Härd, T. *J. Magn. Reson.* **1997**, *126*, 48−57. Engelke, J.; Rüterjans H., *J. Biomol. NMR* **1997**, *9*, 63−78.

(21) Zeng, L.; Fischer, M. W. F.; Zuiderweg, E. R. P. *J. Biomol. NMR* **1996**, *7*, 157−162.

(22) Cordier, F.; Brutscher, B.; Marion, D. *J. Biomol. NMR* **1996**, *7*, 163−168.

Table 1. CO Relaxation at 500 MHz[a]

	R_1 (10^{-2} s^{-1})			R_2 (s^{-1})		
	5 ns	10 ns	15 ns	5 ns	10 ns	15 ns
$\rho_{H\alpha}$	4.02	2.10	1.41	0.391	0.783	1.175
ρ_{HN}	5.06	2.64	1.78	0.493	0.986	1.48
$\rho_{C\alpha}$	11.0	19.3	27.9	0.225	0.450	0.675
ρ_N	3.80	2.11	1.44	0.067	0.134	0.201
ρ_{CSA}	30.3	15.9	10.7	3.31	6.63	9.95
ρ_1, ρ_2	55.4	42.0	43.2	4.49	8.99	13.4
$\eta_{CSAH\alpha}$	−17.2	−9.03	−6.07	−1.97	−3.82	−5.69
η_{CSAHN}	10.8	5.67	3.81	1.24	3.82	3.57
$\eta_{CSAC\alpha}$	−9.21	−4.82	−3.24	−1.05	−2.04	−3.04
η_{CSAN}	4.16	2.17	1.46	0.476	0.920	1.37
$\eta_{H\alpha HN}$	−1.83	−0.959	−0.645	−0.209	−0.405	−0.604
$\eta_{H\alpha C\alpha}$	2.96	1.55	1.04	0.339	0.657	0.979
$\eta_{H\alpha N}$	−1.29	−0.678	−0.456	−0.148	−0.286	−0.427
$\eta_{C\alpha N}$	0.458	0.240	0.162	0.053	0.101	0.151
$\eta_{C\alpha HN}$	−2.52	−1.32	−0.890	−0.288	−0.559	−0.833
η_{NHN}	−2.17	−1.13	−0.764	−0.248	−0.480	−0.716
$\sigma_{H\alpha}$	0.164	0.0818	0.0546			
σ_{HN}	0.206	0.103	0.0687			
$\sigma_{C\alpha}$	−8.15	−17.5	−26.7			
σ_N	2.97	1.68	1.15			

[a] Contributions to the overall relaxation rates are tabulated, e.g., for the C′−Cα dipolar interaction as $\rho_{C\alpha}$. The cross-correlation rates are tabulated, e.g., for the C′−Cα(dipolar)/C′−HN(dipolar) interference as $\eta_{C\alpha HN}$, and for the C′(CSA)/C′−HN(dipolar) interference as η_{CSAHN}. The cross-relaxation rates are tabulated, e.g., for the C′−Cα dipolar interaction, as $\sigma_{C\alpha}$. The calculations are based on the equations in this paper and were carried out for three rotational correlation times as indicated. All order parameters are equal to one. Distances between nuclei and angles between internuclear vectors were obtained for an α-helical conformation from the modeling program InsightII (Molecular Simulations, Inc.). The C′ CSA tensor was here assumed to be axially symmetric, with the principal axis lying in the Cα−C′−N plane making an angle of 157° with the Cα−C′ vector. The anisotropy was taken as −120 ppm.

several residues of the 20 kDa protein flavodoxin of *Escherichia coli*, for which the NMR resonance assignments[23] and crystal structure[24] are known.

Materials and Methods

The NMR data were recorded on *E. coli* flavodoxin, in the oxidized diamagnetic state. The ∼1 mM flavodoxin sample was in 10 mM phosphate buffer at pH 6.2, and was kept at 20 °C during these studies. A 0.5 mL UL-^{13}C,^{15}N-labeled sample was used for ^{15}N relaxation studies, using a Bruker AMX-500 spectrometer, equipped with a 5 mm triple-resonance gradient probe. The ^{15}N relaxation series were obtained using H → ^{15}N NOE, T_1 and $T_{1\rho}$ sequences.[25] The H_2O signal was kept in the +z-direction for the T_1 and $T_{1\rho}$ experiments. To avoid a change in H_2O saturation level by the changing length of the cross-correlation suppression pulse trains[26] as a function of the relaxation measurement delay, these pulses were carried out as a $90_x-\tau-90_x$ sequence, yielding a 0° flip angle of the water signal and a 180° flip angle of the amide protons using a delay τ of 333 μs. The $T_{1\rho}$ experiment used a ^{15}N spin lock field of 2381 Hz placed at the center of the spectrum. The control ^{15}N NOE experiment was measured by keeping the H_2O signal along +z. The ^{15}N relaxation data collection, carried out on the 500 MHz system, took two weeks in total. The exchange contribution to the ^{15}N line width was determined independently with the use of a slightly modified version of the constant time off-resonance $T_{1\rho}$ experiment, as introduced by Akke and Palmer.[27] Five different carrier offsets were used, yielding effective spin-lock fields of 1990−3845 Hz, sampling conformational dynamics on a timescale slower than 40 μs.[28] Eight $T_{1\rho}$ relaxation delays, varying from 8 to 248 ms were used per offset. Total experimental time was 5 days.

The sample was transferred to an 8 mm Shigemi microcell (Shigemi, Inc) for use with a Bruker AMX-600 spectrometer, equipped with an 8 mm Nalorac triple resonance gradient probe. All C′ relaxation measurements were carried out on the 600 MHz system. The Cα→C′ NOE experiment was carried out with the pulse sequence described earlier.[21] Three experiments were collected: (i) with the Cα resonances saturated using Gaussian excitation pulses and ^{1}H resonances saturated using Waltz-16 for 10s; (ii) with the Gaussian saturating field frequency switched to an off-resonance position, equidistant down-field from the 13C′ resonances, while maintaining the ^{1}H saturation; (iii) a control without any saturation. Subtraction of i and ii measures the Cα→C′ NOE while suppressing all H→C′ cross-relaxation and cross-correlation effects. The ratio (i − ii)/iii then gives the desired Cα→C′ NOE difference. Each spectrum took 14 h. The C′ T_1 relaxation was measured with the sequence described before[21] with the Cα and ^{1}H resonances saturated during the relaxation measuring delay, using Gaussian excitation pulses. This was done to eliminate cross-relaxation and cross-correlation effects due to interactions with these nuclei. The C′(CSA)−C′−Cα(dipolar) cross-correlation was measured with the 3D experiment shown in Figure 4. Experimental time was 12 days; see the legend to Figure 4 for experimental details.

All NMR data were processed using Silicon Graphics computer systems, using Felix software (a gift from Hare Research, Inc.). ^{15}N T_1 and $T_{1\rho}$ as well as ^{13}C′ T_1 values were determined from the data using a software package kindly provided by Dr. Nicholson, as well as some in-house simulated annealing algorithms. We used partial integration of cross-peak volumes in order to optimize signal−noise ratios.[29] Modeling of relaxation was carried out on Silicon Graphics workstations, using the software package *Mathematica*, release 3.0.

For ease of data comparison, we adopt in this paper a numbering system that assigns the Cα residue number to all the nuclei of the peptide plane CO−N−NH following that Cα.

Theory

In this work, we study amide nitrogen relaxation, carbonyl relaxation, and the cross-correlation between carbonyl (C′) chemical shift anisotropy (CSA) relaxation and the C′−Cα dipolar interaction. The theory describing N−NH relaxation has been well developed and will not be reproduced here. The reader is referred to Dayie et al.[1]

The longitudinal and transverse relaxation rates of the C′ resonance are, to a good approximation, governed by the C′ chemical shift anisotropy and the dipole−dipole interactions with Cα, Hα, N, and HN (See Figure 1 and Table 1). The rates are formally given by[30]

$$\frac{1}{T_1^{C'}} = c_{C'}^2 F_{J1}^{CSAC'} + d_{C'N}^2 F_{J1}^{C'N} + d_{C'C\alpha}^2 F_{J1}^{C'C\alpha} + d_{C'H\alpha}^2 F_{J1}^{C'H\alpha} + d_{C'HN}^2 F_{J1}^{C'HN} \quad (1)$$

and

$$\frac{1}{T_2^{C'}} = c_{C'}^2 F_{J2}^{CSAC'} + d_{C'N}^2 F_{J2}^{C'N} + d_{C'C\alpha}^2 F_{J2}^{C'C\alpha} + d_{C'H\alpha}^2 F_{J2}^{C'H\alpha} + d_{C'HN}^2 F_{J2}^{C'HN} \quad (2)$$

where the dipolar interaction terms are, for example,

$$d_{C'N}^2 = \frac{1}{8}\left(\frac{\mu_0}{4\pi}\right)^2\left(\frac{h}{2\pi}\right)^2 \gamma_{C'}^2\gamma_N^2\langle r_{C'N}^{-3}\rangle^2 \quad (3)$$

(23) Ponstingl, H.; Otting, G. *Eur. J. Biochem.* **1997**, *244*, 384−399.
(24) Hoover, D. H.; Ludwig, L. L. *Protein Sci.*, submitted for publication.
(25) Dayie, K. T.; Wagner, G *J. Magn. Reson. A* **1994**, *111*, 121−126.
(26) Boyd, J.; Hommel, U.; Campbell, I. D. *Chem. Phys. Lett.* **1990**, *175*, 477−482. Palmer, A. G., III.; Skelton, N. J.; Chazin, W. J.; Wright, P. E.; Rance, M. *Mol. Phys.* **1991**, *75*, 699−712.
(27) Akke, M.; Palmer, A. G., III. *J. Am. Chem. Soc.* **1996**, *118*, 911−912.
(28) Davis, D. G.; Perlman, M. E.; London, R. E. *J. Magn. Reson. B* **1994**, *104*, 266−275.
(29) Rischel, C. *J. Magn. Reson. A* **1995**, *116*, 255−258.
(30) Goldman, M. *Quantum description of high-resolution NMR in liquids*; Clarendon: 1988.

while the CSA interaction term is given by

$$c^2_{C'} = \frac{1}{18}\omega^2_{C'}\Delta\sigma^2\left(1 + \frac{\Delta\eta^2}{3}\right) \quad (4)$$

where

$$\Delta\sigma = \sigma_{11} - \frac{(\sigma_{22} + \sigma_{33})}{2}$$

and

$$\Delta\eta = \frac{(\sigma_{22} - \sigma_{33})}{(\sigma_{11} - \sigma_{iso})}$$

The C′ chemical shift tensor deviates severely from axial symmetry; typical anisotropy values are $\sigma_{11} = 75$ ppm, $\sigma_{22} = 3$ ppm, and $\sigma_{33} = -78$ ppm.[31]

Below, we follow the Lipari and Szabo[11] definitions of the spectral density functions to contain the factor $^2/_5$, giving rise to the numerical factors in eqs 3 and 4 below. The spectral density terms for longitudinal relaxation are, for example,

$$F^{C'N}_{J1} = 6J(\omega_{C'}) + 2J(\omega_{C'} - \omega_N) + 12J(\omega_{C'} + \omega_N) \quad (5)$$

and

$$F^{CSAC'}_{J1} = 6J(\omega_{C'}) \quad (6)$$

while the corresponding terms for transverse relaxation are

$$F^{C'N}_{J2} = 4J(0) + 3J(\omega_{C'}) + 6J(\omega_N) + J(\omega_{C'} - \omega_N) + 6J(\omega_{C'} + \omega_N) \quad (7)$$

and

$$F^{CSAC'}_{J2} = 4J(0) + 3J(\omega_{C'}) \quad (8)$$

The C′ relaxation rates are further influenced by cross-correlation effects, which are a consequence of the fact that different relaxation mechanisms affecting a single nucleus are not independent as the interaction vectors are related to each other by the molecular frame.[32] Cross-correlation rates (R(CC)) may potentially be twice as large as the auto-correlation (or "normal") rates, and certainly may not be neglected. The following equations, which are valid only for overall isotropic motion, show this clearly:

$$R(CC)^{DD-DD}_{C'N-C'H\alpha} = 2\left[\frac{1}{8}\left(\frac{\mu_0}{4\pi}\right)^2\left(\frac{h}{2\pi}\right)^2\right]\gamma_C\gamma_N\gamma_C\gamma_H\langle r_{C'N}{}^{-3}\rangle \times \langle r_{C'H\alpha}{}^{-3}\rangle\frac{1}{2}(3\cos^2\theta - 1)\{6J(\omega_C)\} \quad (9)$$

and

$$R(CC)^{DD-DD}_{C'N-C'H\alpha} = 2\left[\frac{1}{8}\left(\frac{\mu_0}{4\pi}\right)^2\left(\frac{h}{2\pi}\right)^2\right]\gamma_C\gamma_N\gamma_C\gamma_H\langle r_{C'N}{}^{-3}\rangle \times \langle r_{C'H\alpha}{}^{-3}\rangle\frac{1}{2}(3\cos^2\theta - 1)\{4J(0) + 3J(\omega_C)\} \quad (10)$$

for the C′−N dipole−dipole/C′−Hα dipole−dipole cross-correlation on T_1 and T_2, respectively,[33] where θ is the angle between the vectors, and, e.g.,

$$R(CC)^{CSA-DD}_{C'-C'C\alpha} = 2\left[\frac{1}{12}\left(\frac{\mu_0}{4\pi}\right)\left(\frac{h}{2\pi}\right)\right]\omega_{C'}(\sigma_{||} - \sigma_{\perp})\gamma_C\gamma_C\langle r_{C'C\alpha}{}^{-3}\rangle \times \frac{1}{2}(3\cos^2\theta - 1)\{6J(\omega_C)\} \quad (11)$$

and

$$R(CC)^{CSA-DD}_{C'-C'C\alpha} = 2\left[\frac{1}{12}\left(\frac{\mu_0}{4\pi}\right)\left(\frac{h}{2\pi}\right)\right]\omega_{C'}(\sigma_{||} - \sigma_{\perp})\gamma_C\gamma_C\langle r_{C'C\alpha}{}^{-3}\rangle \times \frac{1}{2}(3\cos^2\theta - 1)\{4J(0) + 3J(\omega_C)\} \quad (12)$$

for an axial C′ CSA/C′−Cα dipole−dipole cross-correlation on T_1 and T_2 relaxation, respectively, where θ is the angle between the dipolar vector and the CSA principal axis.[34] The cross correlation for T_2 is expressed for the nonaxial C′ CSA tensor as a sum of two axial tensor cross correlations

$$R(CC)^{CSA-DD}_{C'-C'C\alpha} = 2\left[\frac{1}{12}\left(\frac{\mu_0}{4\pi}\right)\left(\frac{h}{2\pi}\right)\right]\omega_{C'}\gamma_C\gamma_C\langle r_{C'C\alpha}{}^{-3}\rangle \times \left[(\sigma_{11} - \sigma_{33})\frac{1}{2}(3\cos^2\theta_{11} - 1) + (\sigma_{22} - \sigma_{33})\frac{1}{2}(3\cos^2\theta_{22} - 1)\right]\{4J(0) + 3J(\omega_C)\} \quad (13)$$

where θ_{11} and θ_{22} are the angles between the dipolar vector and the σ_{11} axis and σ_{22} axis, respectively. The cross-correlation equations carry an explicit factor of 2 to account for the fact that two cross-products exist for each pair of perturbing Hamiltonians.

The quantities $J(\omega)$ in eqs 9−13 are *cross-correlation spectral densities*, which can differ greatly from the usual auto-correlation spectral densities[35,36] (see below).

Cross-correlations are manifested as different relaxation rates for molecules that have different spin polarization states. For instance, the C′ resonance in molecules with Cα in the $|\alpha\rangle$ state will have a different relaxation rate than the C′ resonance in a molecule with Cα in the $|\beta\rangle$ state as the dipolar field of Cα can either compensate or reinforce the C′ CSA.[37] When the two different ensembles can be discriminated, e.g., through scalar coupling between C′ and Cα, these relaxation differences can be directly measured and related to the above equations (see eqs 45−47). When the different molecules cannot be distinguished, a bi- or multiexponential relaxation of the C′ resonance

(31) Teng, Q. Determination of tensor orientations and the applications in the study of gramicidin A by solid state NMR. Ph.D. Thesis, Florida State University, Tallahassee, FL, 1990.

(32) Fagerness, P. E.; Grant, D. M.; Kuhlmann, K. F.; Mayne, C. L.; Parry, R. B. *J. Chem. Phys.* **1975**, *63*, 2524−2532. Werbelow, L. G.; Grant, D. M. *Adv. Magn. Reson.* **1977**, *9*, 189−301. Vold R. L.; Vold R. R. *Progr. NMR Spectrosc.* **1978**, *12*, 79−133. Werbelow, L. G. In *Nuclear magnetic resonance probes of molecular dynamics*; Tycho, R., Ed.; Kluwer Academic Publisher: New York, 1944; pp 223−263. Kumar, Anil.; Madhu, P. K. *Conc. Magn. Reson.* **1996**, *8*, 139−160.

(33) Dalvit, C.; Bodenhausen, G. *Adv. Nucl. Mag. Reson.* **1990**, *5*, 1−33.

(34) Goldman, M. *J. Magn. Reson.* **1984**, *60*, 437−452.

(35) Daragan, V. A.; Mayo, K. H. *Chem. Phys. Lett.* **1993**, *206*, 393−400. Daragan, V. A.; Kloczewiak M. A.; Mayo, K. H. *Biochemistry* **1993**, *32*, 10580−10590. Daragan, V. A.; Mayo, K. H. *Biochemistry* **1993**, *32*, 11488−11499. Daragan, V. A.; Mayo, K. H. *Progr. NMR Spectrosc.* **1997**, *31*, 63−105.

(36) Daragan, V. A.; Mayo, K. H. *J. Magn. Reson B* **1995**, *107*, 274−278. Daragan, V. A.; Mayo, K. H. *J. Phys. Chem.* **1994**, *98*, 10949−10956. Kay, L. E.; Torchia, D. A. *J. Magn. Reson.* **1991**, *95*, 536−547.

(37) Cuperlovic, M.; Palke, W. E.; Gerig, J. T.; Gray, G. A. *J. Magn. Reson. B.* **1996**, *110*, 26−38. Brüschweiler, R.; Griesinger, C.; Ernst, R. R. *J. Am. Chem. Soc.* **1989**, *111*, 8034−8035. Yang, D.; Ye, C. *Chem. Phys. Lett.* **1991**, *183*, 309−315.

will be observed. Cross-correlations can be suppressed by interchanging the spin states of the Cα spin using π pulses on a time scale fast compared to the macroscopic relaxation rate.[26,38] For the five mechanisms active for C′ relaxation we anticipate 10 different cross-correlations as shown in Table 1.

In addition, at least four longitudinal cross relaxation (σ or NOE) effects between the C′ and the other nuclei Q can be distinguished, given by[34]

$$\sigma_{C'Q} = \frac{1}{8}\left(\frac{\mu_0}{4\pi}\right)^2\left(\frac{h}{2\pi}\right)^2\gamma_{C'}^2\gamma_Q^2\langle r_{C'Q}^{-3}\rangle^2\{12J(\omega_{C'}+\omega_Q) - 2J(\omega_C-\omega_Q)\} \quad (14)$$

where the homonuclear Cα→C′ NOE is by far the largest (see Table 1). The NOEs can be explicitly measured[21] or should otherwise be suppressed in longitudinal relaxation measurements as they cause multiexponential relaxation.[39]

From the above, it is clear that C′ relaxation is governed by many parameters and is thus difficult to analyze. For macromolecules, the spectral density terms are generally thought to reflect sums of global and local motions. We specifically recognize that it is very unlikely that local motions in an anisotropic intramolecular environment can be isotropic. In general, the spectral densities $J(\omega)$ will thus be different for all interactions because each of the interaction vectors point in different directions. Local anisotropic motion about the C′−Cα vector, for example, will not contribute to C′−Cα dipolar relaxation but will certainly cause the tensor elements of the C′ CSA to reorient in space leading to C′ CSA relaxation and averaging. Thus, local anisotropic motions are sensed differently for the different relaxation interactions. One must therefore write independent spectral density functions and order parameters for each interaction (auto-correlation) and for each interaction pair (cross-correlation). This approach is radically different from recently presented work,[20] in which it was assumed that a single order parameter for C′ relaxation would be adequate.

In the following, we give a general derivation that leads to the definition of both auto-correlation order parameters as well as cross-correlation order parameters for CSA−dipolar relaxation effects. The formalism largely follows Lipari and Szabo,[11] Daragan and Mayo,[36] and Brüschweiler and Case.[40] We treat the case of overall isotropic dynamics combined with local anisotropic motion; anisotropic overal motion combined with anisotropic local motion can in principle be treated by combining the material below with theories for overall anisotropic motion.[41−43] However, since these effects would be very difficult to characterize experimentally, we have not included such derivations here.

The time-dependent parts of the correlation functions are, in the laboratory frame, for dipolar and CSA Hamiltonians

$$C_{lab}^{\mathbf{ab}}(t) = \frac{4\pi}{5}\langle Y_{20}(\cos(\theta^{\mathbf{a}}(0)))\cdot Y_{20}(\cos(\theta^{\mathbf{b}}(t)))\rangle_{lab} \quad (15)$$

where

$$Y_{20}\cos(\theta(t)) = \sqrt{\frac{5}{4\pi}}P_2\cos(\theta(t)) \quad (16)$$

and

$$P_2\cos(\theta(t)) = \frac{1}{2}(3\cos^2(\theta(t)) - 1) \quad (17)$$

and $\theta^{\mathbf{a}}(t)$ is the angle between the interaction vector in the Hamiltonian (e.g., the internuclear vector between the dipolar coupled spins, or the principal axis of the CSA tensor) and some arbitrary direction in space.

The cross- and auto-correlation spectral density functions appearing in the equations 1−14 are defined as

$$J_{\mathbf{ab}}(\omega) = \frac{8\pi}{5}\int_0^\infty\langle Y_{20}(\cos(\theta^{\mathbf{a}}(0)))\cdot Y_{20}(\cos(\theta^{\mathbf{b}}(t)))\rangle_{lab}\cos\omega t\,dt \quad (18)$$

The key step to obtain relaxation rates in terms of order parameters is to factor[11] the total correlation function (eq 15) into the overall isotropic motion and the local motion:

$$C_{lab}^{\mathbf{ab}}(t) = \frac{1}{5}\exp(-t/\tau_C)\cdot C_L^{\mathbf{ab}}(t) \quad (19)$$

defining the overall correlation time τ_C, and the local (cross) correlation function

$$C_L^{\mathbf{ab}}(t) = \frac{4\pi}{5}\sum_{m=-2}^{2}\langle Y_{2m}(\vartheta^{\mathbf{a}}(0),\varphi^{\mathbf{a}}(0))\cdot Y_{2m}^*(\vartheta^{\mathbf{b}}(t),\varphi^{\mathbf{b}}(t))\rangle \quad (20)$$

In order to characterize the local motion, one tries to obtain limiting cases for the local correlation function. For $t = 0$ one has

$$C_L^{\mathbf{ab}}(0) = \frac{4\pi}{5}\sum_{m=-2}^{2}Y_{2m}(\vartheta^{\mathbf{a}}(0),\varphi^{\mathbf{a}}(0))\cdot Y_{2m}^*(\vartheta^{\mathbf{b}}(0),\varphi^{\mathbf{b}}(0)) = P_2(\cos\theta_{\mathbf{ab}}) \quad (21)$$

using the addition theorem of spherical harmonics, with $\theta_{\mathbf{ab}}$ the angle between the two interaction vectors. For $t \rightarrow \infty$ one writes, using the following property of correlation functions:

$$\lim_{t\rightarrow\infty}\langle A(t)\cdot B(0)\rangle = \langle A\rangle\langle B\rangle \quad (22)$$

$$C_L^{\mathbf{ab}}(\infty) = S_{\mathbf{ab}}^2 = \frac{4\pi}{5}\sum_{m=-2}^{2}\langle Y_{2m}(\vartheta^{\mathbf{a}},\varphi^{\mathbf{a}})\rangle\langle Y_{2m}^*(\vartheta^{\mathbf{b}},\varphi^{\mathbf{b}})\rangle \quad (23)$$

where $S_{\mathbf{ab}}^2$ is defined as the cross ($\mathbf{a} \neq \mathbf{b}$) or auto ($\mathbf{a} = \mathbf{b}$) correlation order parameter.[36]

Averages such as $\langle Y_{2m}^*(\vartheta^{\mathbf{b}},\varphi^{\mathbf{b}})\rangle$ depend on the local motion $\mathbf{L}^{\mathbf{b}}(\vartheta^{\mathbf{b}},\varphi^{\mathbf{b}})$ and are computed[36] as, e.g.:

$$\langle Y_{2m}^*(\vartheta^{\mathbf{b}},\varphi^{\mathbf{b}})\rangle = \int\int Y_{2m}^*(\vartheta^{\mathbf{b}},\varphi^{\mathbf{b}})\mathbf{L}^{\mathbf{b}}(\vartheta^{\mathbf{b}},\varphi^{\mathbf{b}})\,d\varphi^{\mathbf{b}}\sin(\vartheta^{\mathbf{b}})\,d\vartheta^{\mathbf{b}} \quad (24)$$

This leads to the spectral density $J_{ab}(\omega)$

$$J_{\mathbf{ab}}(\omega) = 2\int_{t=0}^{\infty}C_{lab}^{\mathbf{ab}}(t)\cos\omega t\,dt = \frac{2}{5}\left\{\frac{S_{\mathbf{ab}}^2\tau_c}{1+(\omega\tau_c)^2} + \frac{(P_2(\cos\theta^{\mathbf{ab}}) - S_{\mathbf{ab}}^2)\tau_M}{1+(\omega\tau_M)^2}\right\} \quad (25)$$

(38) Kay, L. E.; Nicholson, L. K.; Delaglio, F.; Bax, A.; Torchia, D. A. *J. Magn. Reson.* **1992**, *97*, 359−375.
(39) Solomon, I. *Phys. Rev.* **1955**, *99*, 559−565.
(40) Brüschweiler, R.; Case, D. A. *Prog. NMR Spectrosc.* **1994**, *26*, 27−58.
(41) Chung, J.; Oldfiled, E.; Thevand, A.; Werbelow, L. *J. Magn. Reson.* **1992**, *100*, 69−81. Werbelow, L. In *Encyclopedia of NMR* 1996; pp 4072−4078.
(42) Zheng, Z.; Czaplicki, J.; Jardetzky, O. *Biochemistry* **1995**, *34*, 5212−5223.
(43) Woessner, D. E. *J. Chem. Phys.* **1962**, *37*, 647−654.

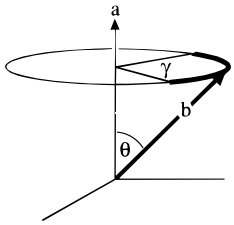

Figure 2. Definition of the parameters used in the motional modeling of this study. Rotational diffusion about vector **a** causes the vector **b** to sweep out a cone of half angle $\theta = \cos^{-1}(\mathbf{a}\cdot\mathbf{b})$. The extent of the motion on this cone is given by the angle γ, defined as 2π for unrestricted rotational diffusion.

with

$$\tau_M = \frac{\tau_c \tau_e}{\tau_c + \tau_e} \tag{26}$$

where τ_e is the correlation time of the dominant local motion.

The function 25 takes the place of the term $^1/_2(3\cos^2\theta - 1)J(\omega)$ in eqs 11−13.

The cross-correlation spectral density function, $J_{\mathbf{ab}}(\omega)$ becomes the familiar "model free" auto-correlation spectral density function[11]

$$J_{\mathbf{aa}}(\omega) = \frac{2}{5}\left\{\frac{S^2_{\mathbf{aa}}\tau_c}{1+(\omega\tau_c)^2} + \frac{(1-S^2_{\mathbf{aa}})\tau_M}{1+(\omega\tau_M)^2}\right\} \tag{27}$$

when $\mathbf{b} = \mathbf{a}$. One is tempted to view eq 25 as

$$J_{\mathbf{ab}}(\omega) = \frac{2}{5}P_2(\cos\theta^{\mathbf{ab}})\left\{\frac{S^2_{\mathbf{aa}}\tau_c}{1+(\omega\tau_c)^2} + \frac{(1-S^2_{\mathbf{aa}})\tau_M}{1+(\omega\tau_M)^2}\right\} \tag{28}$$

merely identifying

$$S^2_{\mathbf{ab}} = P_2(\cos\theta^{\mathbf{ab}})S^2_{\mathbf{aa}} = P_2(\cos\theta^{\mathbf{ab}})S^2_{\mathbf{bb}} \tag{29}$$

This interpretation seems to be supported by the fact that for no internal motion

$$S^2_{\mathbf{ab}}(\max) = P_2(\cos\theta^{\mathbf{ab}}) \tag{30}$$

as follows from eq 21.

However, eq 29 can only be generally valid for isotropic local motions, or when vectors **a** and **b** are colinear. Only then can knowledge of motional freedom or restriction of vector **a** lead to knowledge of the motional freedom or restriction of a vector **b**. As it is very unlikely that local motions are isotropic, we reject the interpretation of the cross-correlation order parameter as given in eq 29. Instead, we will simply interpret and calculate the cross-correlation order parameter as a measure of the ability of the local motion to perturb the cross-correlation due to isotropic tumbling.

Following Daragan and Mayo,[36] we model the local anisotropic motions as (limited) rotational diffusion around unique vectors. In this definition, motion about the vector **a** will not affect the interaction along direction *a*, but reorients the vector **b** on the surface of a cone with half angle $\cos^{-1}(\mathbf{a}\cdot\mathbf{b})$ and thus affects the relaxation associated with the motion of vector **b**. The parameter γ determines the extent of this rotation; $\gamma = 2\pi$ defines unrestricted rotation around direction *a* resulting in unrestricted rotational diffusion on a cone for vector **b** (see Figure 2). This model is well suited to describe (local) anisotropic motion while retaining proper geometric relations between the different vectors in the molecule. The motional model is parametrized by γ and its effect on the averaging of the spherical harmonics is computed with equations such as eq 24. Auto- and cross-correlation order parameters are then easily computed from eq 23, and auto- and cross-correlation spectral densities follow from eq 25.

In this study we consider the reorientations of the vectors C′(*i*)−Cα(*i*), N(*i*+1)−H(*i*+1) and the different axes of the CSA tensor of C′(*i*). These vectors are all rigidly interrelated by the peptide plane connecting residues *i* and *i*+1. For example, local rotational diffusion around the direction of the N−NH vector immediately implies that the C′−Cα sweeps a cone of half angle 58°. This motion would generate variation in the C′−Cα dipolar interaction, thus affecting the dominant $J(\omega = 0)$ (averaging) and $J(\omega \neq 0)$ (transition) terms; it will thus affect the C′−Cα dipolar interaction order parameter. This motion will not generate variation in the N−NH dipolar interaction and will thus leave the N−NH order parameter unaffected. Implicitly this also means that this motion quenches cross-correlation between these mechanisms. As a result the cross-correlation as dictated by the overall molecular tumbling remains unaffected [$S^2_{\mathbf{ab}} = P_2\cos(\theta_{\mathbf{ab}})$].

We consider three different and orthogonal motions, for convenience chosen along the axes of the C′ chemical shift tensor (see Figure 1). The consequences of these motions on the C′−Cα dipolar relaxation order parameter ($S^2_{C'-C\alpha}$), the N−NH dipolar (and CSA) relaxation order parameter (S^2_{N-NH}) as well as on the C′−Cα dipole−dipole/C′ CSA cross-correlation (*R*(CC), measured in hertz) are shown pairwise in Figure 3A−C. The parts of the figure, called motional restriction maps,[36] clearly indicate that different motions affect the different order parameters in different ways. Figure 3A shows that motion about or parallel to σ_{22} does not affect S^2_{N-NH} but has a large effect on $S^2_{C'-C\alpha}$ as described already. Conversely, motion along σ_{11} leaves $S^2_{C'-C\alpha}$ basically unchanged but affects S^2_{N-NH} strongly. Motion around σ_{33} has approximately equal effects on $S^2_{C'-C\alpha}$ and S^2_{N-NH}, but, from Figure 3A alone, can not be distinguished from motion around any vector in a plane perpendicular to the peptide plane, bisecting the angle between the C′−Cα and N−NH vectors. This includes the so called "in-plane" vector, the vector in the peptide plane that bisects the angle between the σ_{11} and σ_{22} vectors. Also, motion along σ_{33} cannot be distinguished from a "symmetric" local motion in which the N−NH and C′−Cα vectors are reoriented to the same extent. Such motion, indicated by "ISO" in Figure 3, represents what might be expected in a preliminary comparison of N−NH and C′ relaxation order parameters.

Ideally, one would like to have experimental access to an interaction vector perpendicular to the peptide plane in order to distinguish between these cases. Such a vector is available in the σ_{33} of the CSA, and we elect to measure it through the cross-correlation effects with the C′−Cα dipolar relaxation. One may also try to measure the CSA directly from C′ $T_{1\rho}$ which is dominated by the CSA relaxation (see Table 1). However, $T_{1\rho}$, as any transverse measurement, is also affected by chemical exchange, which can complicate matters.

Figure 3B shows that the effect of true motion about σ_{33} and motion about the in-plane vector can be readily distinguished. In Figure 3C the distinction is made even more clearly: the cross-correlation resulting from a motion about σ_{33} almost coincides with that of motion around the σ_{11} vector while the effect of motion about the in-plane vector coincides with the σ_{22} vector. Thus, random correlated motions, motion about the in-plane vector, and motion about vectors out of the peptide plane (σ_{33} type), which are indistinguishable based on Figure 3A alone, can be distinguished using Figure 3, parts B and C. The effects of different local motions on the cross-correlation

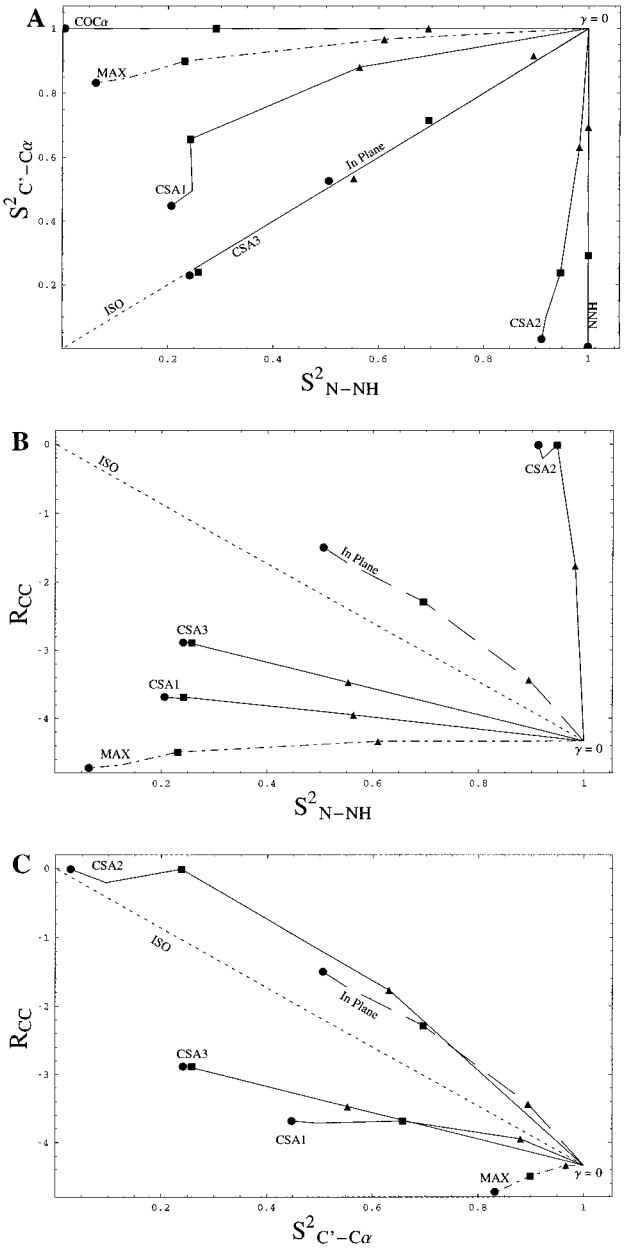

Figure 3. Theoretical behavior of the order parameters for different motions of the peptide plane. Solid lines (CSA1, CSA2, CSA3) indicate motion about axes defined along the principal axes σ_{11}, σ_{22}, and σ_{33}, respectively, of the average C′ CSA tensor as defined in Table 2. The long dashed line (in plane) indicates motion about a vector in the peptide plane bisecting the C′−Cα and N−NH axes. The long−short dashed line (max) indicates motion about that axis which results in the maximum cross-correlation relaxation rate. The short dashed line (iso) indicates a motion in which all internuclear vectors are reoriented to the same extent. In all plots, $\gamma = 90°$, $\gamma = 180°$, and $\gamma = 360°$ are indicated by ▲, ■, and ●, respectively: (A) the order parameters $S^2_{C'-C\alpha}$ and S^2_{N-NH}. The limiting cases of motion about the C′−Cα and N−NH axes are indicated by the lines COCA and NNH respectively; (B) the C′(CSA)/C′−Cα(dipolar) cross-correlation rate and the order parameter S^2_{N-NH}; and (C) the C′(CSA)/C′−Cα(dipolar) cross-correlation rate and the order parameter $S^2_{C'-C\alpha}$.

are less easily visualized than those for the simple interaction vectors. First we realize that in the absence of local motion cross-correlation occurs with a value dictated by the angle between the C′−Cα and CSA axes vectors (see eqs 11−13 and 25). Local motions generally reduce the cross-correlation; this is the case when C′−Cα dipolar and CSA relaxation both sense the local motion equally; the effect is that of a fast isotropic motion which directly reduces τ_c and hence the numerical value of the overall cross-correlation (eqs 13 and 25). In contrast, a motion that leaves unaffected one of the interaction vectors of the cross-correlation is an uncorrelated motion for these vectors. Hence, such local motion will not be cross-correlated and will thus not affect the *existing* cross-correlation associated with the random tumbling of the entire molecule. Thus these local motions leave the value of the cross-correlation unchanged. For instance, local motion around C′−Cα (close to σ_{11}) has little effect on the total cross-correlation (see Figure 3, parts B and C). In fact, if the motional axis coincides exactly with the C′−Cα axis, there is no effect on the cross-correlation. This special case maps as *a single point* at the "origin" $S^2_{C'-C\alpha} = 1$ in Figure 3C since neither auto- or cross-correlation are affected by the motion. Due to the fact that the C′ CSA is not axially symmetric, the effects of motions exactly around the different CSA axes can give unexpected results.

The motional restriction maps[36] in Figure 3A−C were computed by using eq 24 and modeling the motions by integrating and normalizing over five different extents γ as indicated. This is a coarse digitization, resulting in the somewhat jerky behavior of the lines at large values of γ. Most of the anisotropic motions cannot fully quench the order parameters and/or cross-correlation, as they may retain a finite projection of the interaction parameter(s) on the motional axis. Fully isotropic local motion, unlikely in cases of large amplitude, can quench all order. All order parameters are reduced in concerted fashion with increasing extent of motion; this is also true for the cross-correlation order parameter, which for isotropic motion can rigorously be interpreted as a scaled version of the general order parameter (cf. eq 28). Isotropic motions can thus be represented with straight dashed lines from coordinates 1,1 to 0,0 in Figure 3A and 1,−4.1 to 0,0 in Figure 3B,C.

Experimental Design and Results

Our experimental approach is to design and apply experiments that will extract specific interactions or pairs of interactions that influence C′ relaxation. Recently, we published an experiment to isolate the C′−Cα dipolar interaction by measuring the steady state Cα→C′ homonuclear NOE and C′ T_1 relaxation.[21] The steady-state Cα→C′ NOE measurement is made with the "second half" of a 2D HNCO experiment, recording the coherence pathway C′ → N(t1) → H(t2), once with Cα presaturation (10 s) with continuous saturation of protons (experiment *I*), once with the carbon presaturation field moved to an off-resonance position with continuous saturation of protons (experiment *I*′), and once without any cw rf field (experiment I_0). With the proton saturation, all large cross-correlations and cross-relaxations involving protons are effectively quenched. Cross-correlation and cross-relaxation due to C′−N interactions are present in this setup, but can be neglected as the largest is only 3% of the total T_1 relaxation rate (see Table 1). The C′(CSA)/C′N(dipolar) cross-correlation (the largest term) only affects the single-quantum C′ relaxation pathways, present in ρ but not in σ. We obtain the C′−Cα cross relaxation rate σ from $\sigma = \rho\,(I - I')/I_0$, where ρ is the full C′ T_1 relaxation rate, given by eq 1. ρ is measured independently from an HNCO experiment in which a longitudinal C′ relaxation period is inserted.[21] The T_1 relaxation experiment is also carried out with proton and Cα saturation in order to quench all large cross relaxations and cross-correlations. The cross-correlation due to C′−N interaction was not suppressed here either, allowing the potential minimal error in T_1 relaxation rate determination to be divided away in the determination of σ. Nevertheless, the Cα → C′ NOE experiment recorded with these precautions is still not free of unwanted contributions. Cα irradiation also introduces the NOE Cα(i+1)

→ C′(*i*) in addition to the desired NOE Cα(*i*) → C′(*i*); also Cβ(*i*) and Cβ(*i*+1) are (partially) saturated and contribute to the observed steady-state NOE, in a purely additive way. Individually, such nondesirable contributions are only 1−3% of the steady-state NOE; but together they can contribute up to 10% and can thus not be neglected. We can compute these contributions precisely for each site since the coordinates for flavodoxin are available.[24] In situations where no (precise) structure is known, one should use a mean-field correction of 10% for all residues, except for glycine which needs a correction of only 4% because it is lacking the β-carbon. With these precautions and corrections, we obtain the Cα(*i*)→ C′(*i*) cross-relaxation rate σ, which can then be related to the spectral density functions $J(0)$ and $J(2\omega_C)$, exclusively for the C′−Cα vector, according to eq 14. We obtain[21] the auto-correlation order parameter for this vector to a very good approximation from the equation

$$S^2_{C'-C\alpha} = -10\left(\frac{4\pi}{\mu_0}\right)^2\left(\frac{2\pi}{h}\right)^2\left(\frac{r^3_{C'\,C\alpha}}{\gamma^2_C}\right)^2 \sigma_{C'\,C\alpha}\tau_C \qquad (31)$$

From ^{15}N $T_1/T_{1\rho}$ ratio and H → N steady-state NOE we obtain a rotational correlation time τ_c of 14 ns, assuming an average S^2_{N-NH} of 0.8 and τ_e = 100 ps for the 20 kDa flavodoxin molecule (at 20 °C). The ratio of the three components of the moment of inertia tensor[42] as calculated from the crystal structure[24] of flavodoxin are 1.0:1.17:1.45 (without the last ten residues that are clearly unstructured). From this we compute, using Woessner's classical work[43] that the $J(0)$ spectral densities along these three directions have the ratios 1.0:1.04:1.14. We conclude that flavodoxin can be viewed as an isotropically tumbling molecule characterized by a single correlation time to a good approximation. The order parameter for the C′−Cα vector as a function of residue number is given in the supplemenary material, and is plotted in a different fashion in Figure 6A,C. The data has quite high precision (see Figure 6A); however, the accuracy of all order parameters is dictated by the C′−Cα distance and the correlation time. We have used a C′−Cα distance of 1.52 Å, an average of several sources. C′−Cα bond-stretch vibrations are too small to significantly affect this distance even when averaged with r^{-6} weighting (S. Krimm, personal communication). We estimate the accuracy of the overall rotational correlation time as obtained from ^{15}N relaxation data to be not better than 10%, but since this affects all data equally, it will not interfere with our data interpretation.

The nitrogen relaxation data was analyzed in terms of the conventional model-free approach as follows. The value of the NOE was used to define a set of ordered residues allowing the calculation of τ_c from $T_1/T_{1\rho}$ ratios. The $T_1/T_{1\rho}$ ratios that differ from the average value by more than a standard deviation were eliminated, and τ_c was subsequently recalculated from the reduced ensemble. Limited signal-to-noise ratio, especially in the NOE data, prohibits us from obtaining reliable values of τ_e, the local motion correlation time. Order parameters were therefore calculated from the relaxation parameter that is the least sensitive to the frequency of local motions, i.e. the R_2 relaxation rate. In order to identify potential exchange contributions R_{ex} to the R_2 rates, we measured τ_{ex} directly using the equation[28]

$$R_{ex} = (\delta\omega)^2 p_A p_B \frac{\tau_{ex}}{1+\tau^2_{ex}\omega^2_e} \qquad (32)$$

by varying the effective spinlock field ω_e as described by Akke and Palmer,[27] where $\delta\omega$ is the exchange shift difference and where p_A and p_B are the time fractions spent in conformations A and B. The effective spinlock field was varied between 13 000 and 26 000 rad/s. It was found that the transverse relaxation rates of the large majority of the ^{15}N resonances of flavodoxin are not affected by changes in effective spinlock field strength in this range and at the conditions of the high-sensitivity $T_{1\rho}$ experiment used in conjunction with the T_1 and NOE experiments (rf field strength, ω_{rf} = 15 000 rad/s). Change of apparent relaxation rates as a function of rf field strength was detected for several residues. These changes disclosed the presence of exchange broadening for the ^{15}N resonances of residues 4, 18, 27, 34, 40, 51, 52, 67, 73, 75, 91, 92,98, 104, 111, 116, 120, 121, 125, 143, 147 and 155 (^{15}N numbered as the Cα of the previous residue); the data for these residues was deleted from all figures and tables in this paper. All other R_{ex} values were taken to be 0 Hz (see the Discussion for range of validity). The exchange-free R_2 rate formally still needs correction for R_1 relaxation contribution according to the equation[28]

$$R_{2\,app} = R_{1\rho}\sin^2\theta + R_1\cos^2\theta \qquad (33)$$

where θ is the angle given by $\tan^{-1}(\omega_{rf}/\Delta\omega)$, with $\Delta\omega$ the individual resonance offset for each ^{15}N resonance. At the conditions used, θ is at least 77° (10 ppm offset) for a maximum 5% underestimation of the true T_2 relaxation rate. We thus have to very good approximation $S^2_{N-NH} = R_{2\,app}/R_{1\rho(calc)}$ where $R_{1\rho(calc)}$ is given by eqs 2 and 7, using the appropriate parameters for ^{15}N relaxation (r_{N-NH} = 1.02 Å and $\Delta\sigma_N$ = −160 ppm)[5] and a rotational correlation time of 14 ns obtained as described above. The resulting order parameters S^2_{N-NH} describing the reorientational dynamics of the N−NH vectors is plotted as function of residue number in the Supporting Information, and in conjunction with other relaxation parameters in Figure 6A,B, where the precision is also indicated.

The ^{15}N relaxation data were recorded using the same C,N-labeled protein as used for the C′ relaxation measurements in order to avoid possible changes in τ_c as a result of different apparent viscosities for two different samples. The effects of neighboring ^{13}C nuclei on the ^{15}N relaxation can be safely neglected (less than 1%). This analysis yields an order parameter that is actually a combined order parameter for ^{15}N CSA principal axis and the N−NH bond reorientation. However, since the ^{15}N CSA tensor principal axis and the N−NH dipole−dipole vector diverge by only 17°, one may approximate this by a single order parameter associated with the N−NH bond vector reorientational dynamics.[44]

In principle, one could proceed to measuring more relaxation parameters associated with single vectors for the Cα−C′−N(H)−Cα moiety. The more information that is obtained concerning the reorientation of different internuclear vectors associated with the peptide plane, the better the motion can be characterized. Possible candidates are C′→N NOE, detected on NH and Cα→N NOE detected on NH as well, but these effects are very small (see Table 1) and difficult to measure. Therefore we chose to obtain additional relaxation parameters by measuring cross-correlations in relaxation. Cross-correlations between relaxation mechanisms report on the order parameters of two vectors simultaneously. Provided that these two vectors are rigidly affixed to the Cα−C′−N(H)−Cα moiety, they report on the motion of that moiety and can thus be interpreted in terms of motions of the peptide plane. We focus here on two of the largest R_2 relaxation mechanisms for the C′ nucleus: the C′ CSA relaxation and the C′−Cα dipole−dipole interaction (see Table 1). The C′ T_2 relaxation characteristics for an ideal

(44) Tjandra, N.; Szabo, A.; Bax, A. *J. Am. Chem. Soc.* **1996**, *118*, 6986−6991.

two-spin system in the two ensembles of molecules which differ in Cα polarization is given by (combining results of Goldman[34] and Kay et al.[38]):

$$\frac{dI^+S_\alpha}{dt} = -\left(R_{av} + k_{ex} + i\frac{J_{IS}}{2} + R(CC)\right)I^+S_\alpha - (R_{dif} - k_{ex})I^+S_\beta \quad (34)$$

$$\frac{dI^+S_\beta}{dt} = -\left(R_{av} + k_{ex} - i\frac{J_{IS}}{2} - R(CC)\right)I^+S_\beta - (R_{dif} - k_{ex})I^+S_\alpha \quad (35)$$

where I^+S_α and I^+S_β are the two transitions of the I doublet (C′ spin), J_{IS} the scalar coupling, R_{av} being the average, and R_{dif} being half the difference between the T_2 relaxation rates of in-phase and antiphase I coherence. k_{ex} is half the exchange rate between I^+S_α and I^+S_β caused by spontaneous S spin flaps. This term can in principle average out the relaxation differences between the doublet components, especially in T_1 or T_2 relaxation where the scalar couplings are insufficiently suppressed.[38]

For the T_2 relaxation measured here we are interested in the case where R_{av}, $k_{ex} \ll J_{IS}/2$. Then, two doublet components are observed ("slow exchange" with respect to the S spin flip rate) which both have a Lorentzian line shape, but which have different line widths given by

$$R_2^{I+S\alpha} = R_{av} + k_{ex} - R(CC) \quad (36)$$

and

$$R_2^{I+S\beta} = R_{av} + k_{ex} + R(CC) \quad (37)$$

This cross-correlation rate, R(CC), can be easily measured because of the 54 Hz C′−Cα scalar coupling that separates the C′ resonances of the two ensembles. We have measured the T_1 relaxation of Cα in protonated molecules for the similarly sized molecule T4 lysozyme (19.5 kDa). Values in the range 0.5−1 s^{-1} were found, clearly much smaller than the scalar coupling. In this limit, the Cα spin flips only give rise to equal lifetime broadening on both doublet components (first terms of eqs 34 and 35) and the relaxation behavior of each line is given by eqs 36 and 37.

The sequence used to measure the T_2 cross-correlation between the C′ CSA and the C′−Cα dipolar relaxation is shown in Figure 4. This is a HNCO experiment, in which the Cα−C′ scalar coupling is operative during the C′ evolution time. Since this is a constant-time experiment, the differences in R_2 for the two C′ doublet components as given by eqs 36 and 37 result in different amplitudes for the two components. The amplitudes A are, including all possible relaxation mechanisms:

$$A^{C'}_{C\alpha=\alpha} = \exp(-(\sum R_2 + R_2^* + R_{ex} + \sum J_{unres} + R(CC)^{C'-C\alpha/CSA} + R(CC)^{C'-C\alpha/C'-H\alpha} + R(CC)^{C'-C\alpha/C'-HN} + R(CC)^{C'-C\alpha/C'-N} + \sum_{other} R(CC) + \sum k_{ex})T) \quad (38)$$

$$A^{C'}_{C\alpha=\beta} = \exp(-(\sum R_2 + R_2^* + R_{ex} + \sum J_{unres} - R(CC)^{C'-C\alpha/CSA} - R(CC)^{C'-C\alpha/C'-H\alpha} - R(CC)^{C'-C\alpha/C'-HN} - R(CC)^{C'-C\alpha/C'-N} + \sum_{other} R(CC) + \sum k_{ex})T) \quad (39)$$

where $\sum R_2$, R_2^*, R_{ex} and $\sum J_{unres}$ are all transverse relaxation processes, inhomogeneous broadening, chemical exchange broadening, and unresolved scalar couplings respectively, and where the R(CC) terms represent the different cross-correlations and where $\sum k_{ex}$ are the different mechanisms interchanging the multiplet components (e.g., Cα T_1 relaxation).

By decoupling HN and Hα during the C′ constant time period as shown in Figure 4, all cross-correlations involving H nuclei are averaged out or are the same for both C′−Cα doublet components. The C′−N(dipolar)/C′(CSA) cross-correlation and the C′−N(dipolar)/C′−Cα(dipolar) cross-correlations remain active in this experiment. The C′−N(dipolar)/C′(CSA) cross-correlation is the same for both C′−Cα doublet components and is divided out below, while the C′−N(dipolar)/C′−Cα-(dipolar) cross-correlations can have a maximum magnitude of only 0.15 Hz (Table 1) and is partially averaged because of the changing position of the ^{15}N π pulse. We obtain otherwise rigorously, by taking the ratio of the intensities of the two components:

$$R(CC)_{C'-C\alpha/C'CSA} = -\frac{1}{2T}\ln\frac{A^{C'}_{C\alpha=\alpha}}{A^{C'}_{C\alpha=\beta}} \quad (40)$$

as the plethora of relaxation and broadening mechanisms in eqs 38 and 39 common to the two doublet lines cancels. We compute that the scrambled C′−N(dipolar)/C′−Cα(dipolar) cross-correlation introduces an error of at most 1% on this ratio at the experimental conditions.

We record the cross-correlation experiment as a three-dimensional sequence, as spectral resolution in the NH and C′H planes is limited for flavodoxin. In addition, one records a doublet for each amino acid, thus making the overlap problem worse. Cross sections through C′−Cα doublets on individual ^{15}N planes taken from the 3D data set are shown in Figure 5. We observe that the sensitivity is adequate to quantify the individual doublet peaks with a precision of 4% (signal/noise 25:1) leaving a typical error of ±7% for the ratio expressed in eq 40. The figure illustrates that very different cross-correlation rates are found for different residues. Different tuning of the H refocusing delays in the experiment of Figure 4 would allow the observation of cross-correlations between the $C_{\beta/\gamma}$−$C_{\gamma/\delta}$O-(dipolar) and $C_{\gamma/\delta}$O(CSA) of asparagines and glutamines, respectively. A compilation of the C′−Cα(dipolar)/C′(CSA) cross-correlations for flavodoxin is given in the Supporting Information. The data is given in conjunction with other relaxation parameters in Figure 6B,C.

Discussion

The concurrent measurement of N−NH and C′−Cα relaxation is a logical step forward from measuring only N−NH relaxation for the experimental determination of protein back bone dynamics. Both N−NH and C′−Cα relaxation methods measure the reorientational dynamics of a single but different vector characterized by an order parameter. Both vectors are associated with a single peptide plane. The N−NH and C′−Cα order parameters for flavodoxin are plotted against each other in Figure 6A. It is immediately apparent that the two order parameters show very poor correlation. Typical error ranges, determined as described in the Supporting Information are shown in Figures 6A−C, demonstrating that the lack of correlation is not due to experimental uncertainties.

Inaccuracy in the determination of the overall rotational correlation time τ_c affects both order parameters identically and, therefore, does not change the lack of correlation between them. As outlined above, we obtain that spectral densities can differ by at most 14% for vectors pointing in directions differing by 90° in the slightly anisotropic flavodoxin. As C′−Cα and N−NH vectors of a single peptide plane differ by 58°, the differences in $J(0)$ between these directions can be only roughly

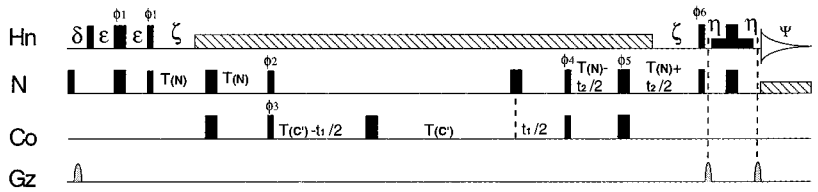

Figure 4. Pulse sequence used for the measurement of the C′(CSA)/C′−Cα(dipolar) cross-correlation, using constant time evolution periods in both the ^{15}N and ^{13}C' dimensions: T(N) = 12.1 ms, T(C′) = 25.14 ms. Thin and thick bars represent 90° and 180° pulses, respectively. All ^{13}C pulses were square and C′ selective. Short solid bars represent selective ^{1}H pulses for watergate water suppression. The following 90° pulse lengths (in microseconds) were used: ^{1}H = 13.76, $^{1}H_{sel}$ = 1000, ^{15}N = 60, $^{13}C'_{sel}$ = 55. Cross-hatched bars indicate WALTZ16 decoupling sequences of field strengths: ^{1}H = 5 kHz, ^{15}N = 833 Hz. All pulses were phase x unless indicated: $\phi_1 = (y)$, $\phi_2 = (x\ x\ -x\ -x)$, $\phi_3 = (x\ -x\ x\ -x)$, $\phi_5 = 4\times(x)4\times(-x)$, $\phi_6 = (-x)$, $\psi = (x\ -x)$. Phases ϕ_3 and ϕ_4 were incremented for States-TPPI quadrature detection. Three 1 ms sine-bell-shaped z-field gradients were used with the following field strengths: 20, 40, and 40 G/cm. Delays (in milliseconds)were as follows: $\delta = 10$, $\epsilon = 2.4$, $\zeta = 5.55$, and $\eta = 1.4$ (η + gradient = ϵ). A total relaxation delay of 1.25 s was used. The acquisition times in the ^{1}H, ^{15}N, and ^{13}C dimensions were 204.8, 49, and 24 ms, respectively. Eight scans per FID were collected. This experiment was then repeated a total of six times for a total experiment time of 300 h. The six data sets were coadded into a single three-dimensional spectrum. The sample was 1.0 mM *E. coli* flavodoxin (20 kDa) at 20 °C and pH 6.2 in a 10 mM phosphate buffer. The data was collected on a Bruker AMX-600 spectrometer, using a 8 mm Nalorac triple resonance gradient probe. The sequence was performed without gradient-selected sensitivity enhancement[48] to avoid excessive ^{15}N rf power deposition in the sample.

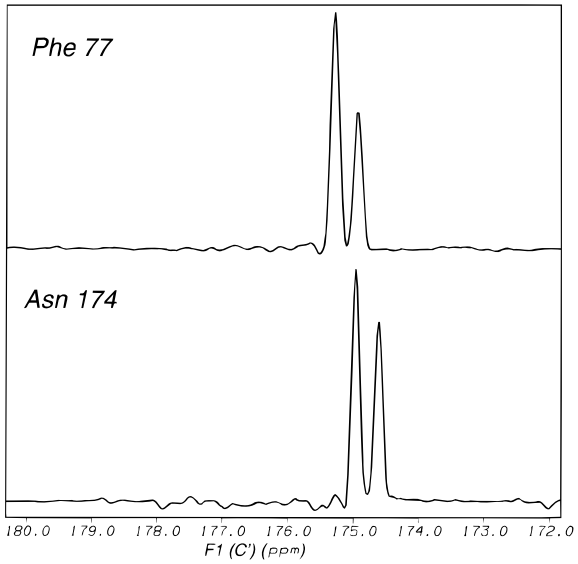

Figure 5. Representative cross sections parallel to the F_1 (C′) axis through the 3D cross-correlation data, for residues 74 and 174. The coupling $^{1}J_{C'-C\alpha}$ is seen to be well resolved. The typical signal to noise ratio, computed as 2.5 × peak height/peak−peak noise, was 25:1.

half the maximum, i.e., 7%. Anisotropic *overall* motion can thus not account for the apparent scatter in the data. As described in the results, we have eliminated the data for those residues for which nitrogen chemical exchange broadening could be measured. Exchange processes slower than 10^{-4} s are completely quenched or would vary detectably with the effective spin-lock field varying between 2000 and 4000 Hz for exchange shift differences ($\delta\omega$) smaller than 6 ppm. Exchange processes faster than 10^{-6} s never give rise to R_{ex} rates larger than 1 Hz for $\delta\omega$ < 6 ppm, and would thus generate at most a small error on the average R_2 rate of 16 s^{-1} obtained for flavodoxin. The only possible exchange contribution that would go undetected in the variable $T_{1\rho}$ experiments, and thus in the data retained by us, are exchange processes around 3 × 10^6 Hz with $\delta\omega$ around 6 ppm. Such processes would give rise to an approximately 3 Hz R_{ex} at all spin lock fields used experimentally. We assume here that it is very unlikely that such conditions would exist for *all* ^{15}N resonances that have a larger apparent S^2_{N-NH} than $S^2_{C'-C\alpha}$. Thus, we conclude that the lack of correlation between the order parameters cannot be explained by exchange contributions to the ^{15}N data. In addition, "devilish" exchange broadening of 3 × 10^6 Hz with shift differences around 6 ppm can, of course, never explain the S^2_{N-NH} values which are *smaller* than the $S^2_{C'-C\alpha}$ values observed, Figure 6A. We have not corrected the N−NH $R_{1\rho}$ data for T_1 contribution (eq 33) as its effect is at most 4% for a 10 ppm offset from the carrier.

We have extensively discussed sources of inaccuracy and imprecision in the determination of the order parameters $S^2_{C'-C\alpha}$ in the Results. All significant complications of cross-correlation and cross-relaxation in our source Cα→C′ NOE and C′ T_1 data have been eliminated. The precision of the resulting $S^2_{C'-C\alpha}$ data is thus overwhelmingly given by the error introduced by noise in the spectral data. The final accuracy of the $S^2_{C'-C\alpha}$ data is governed by the precision of the determination of the overall correlation time; this does however affect all order parameters identically as already mentioned above.

Believing to have eliminated or corrected for all possible sources of scatter in the relaxation data obtained for *E. coli* flavodoxin, we propose that anisotropic *local* motions are responsible for the lack of correlation between S^2_{N-NH} and $S^2_{C'-C\alpha}$ values. The motions experienced by the vectors N−NH and C′−Cα is a summation of the molecular reorientation, individual bond librations and local motion of the peptide plane. Small bond-angle librations may be independent for the two vectors and could in principle account for the lack of correlation. These librations are thought to reduce the order parameter of the N−NH vector only to ∼0.85; by assuming the same to be true for the C′−Cα vector, one may accept that the lack of correlation between both order parameters for $S^2_{C'-C\alpha}$ and S^2_{N-NH} both exceeding 0.85 is to be expected. Smaller order parameters should report on more substantial (pseudo) movements, such as anisotropic rotation of a non-globular protein, and major reorientations of the peptide plane. These motions would be manifested through different $S^2_{C'-C\alpha}$ and S^2_{N-NH} order parameters as the C′−Cα and N−NH vectors make an angle of 58° with each other. In the case when overall anisotropy can be neglected (as for flavodoxin) anisotropic motions must originate from reorientations of (a region of) the peptide planes. *It should be stressed here that such an anisotropic motion is not necessarily around a local axis but can be around any global axis parallel to that local axis, and might thus report on correlated hinge motions of entire peptide surface loops or elements of secondary structure (semilocal motion).*

In Figure 6A, we observe an interesting feature for the residues 156−162, which all have a significantly larger S^2_{N-NH} than $S^2_{C'-C\alpha}$ value. This is compatible with rotational dynamics along the σ_{22} axis, parallel to the N−NH and C′O

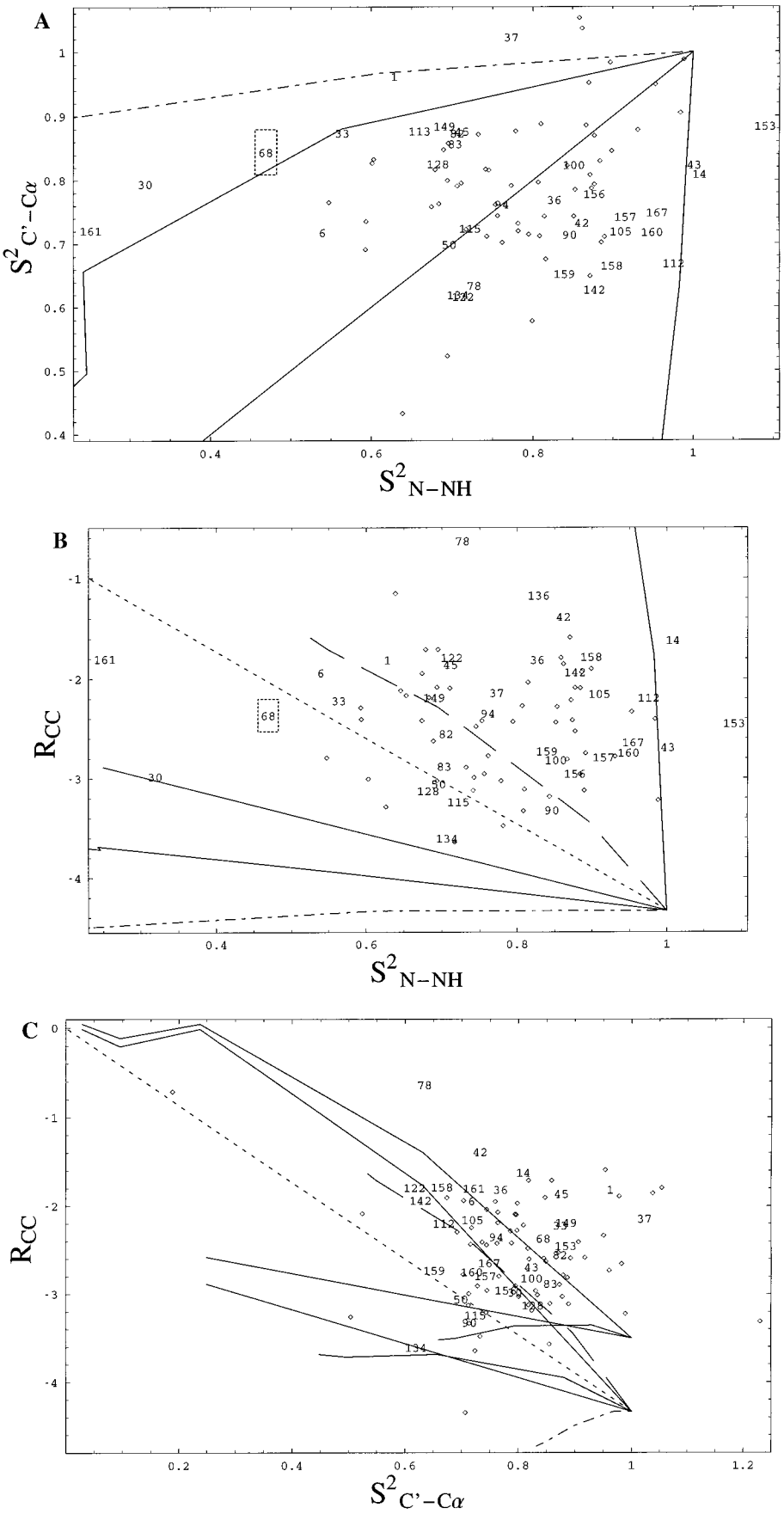

Figure 6. Pairwise presentation of experimental relaxation data for *E. coli* flavodoxin. Motional models and motional extents are as in Figure 3: (A) the order parameters $S^2_{C'-C\alpha}$ and S^2_{N-NH}; the box indicates typical experimental error exemplified for residue 68; (B) the C′(CSA)/C′−Cα-(dipolar) cross-correlation rate and the order parameter S^2_{N-NH}; (C) the C′(CSA)/C′−Cα(dipolar) cross-correlation rate and the order parameter $S^2_{C'-C\alpha}$. In panel C, theoretical curves are shown for both the average C′−CSA tensor described in Table 2 (lower curves) and for the valine C′ CSA tensor given by Teng et al.[46]

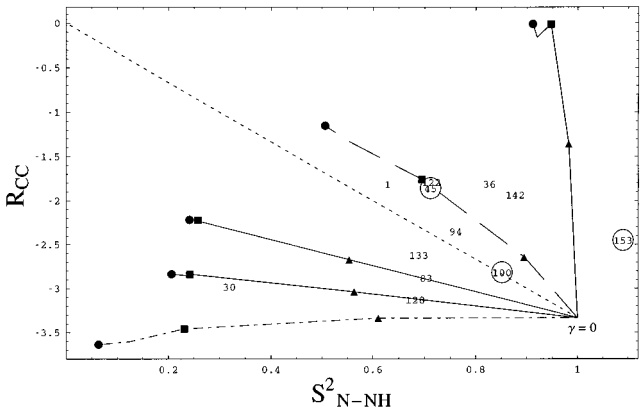

Figure 7. The C′(CSA)/C′−Cα(dipolar) cross-correlation rate and the order parameter S^2_{N-NH} for the peptide planes following alanyl residues in *E. coli* flavodoxin. Motional models and motional extents are as in Figure 3. Residues in α-helical environments are circled. The theoretical model lines as shown in Figure 6C were shifted upward as to better fit the experimental data spread (see text).

bond vectors (see Figure 3a). Inspection of the flavodoxin structure reveals that these residues are part of a single α-helix. Concerted motion of the entire helix around the helical axis (parallel to N−NH and C′O bond vectors) is thus compatible with these observations. As we explain elsewhere,[47] this rotational motion is quite possible for this helix, as it is peripheral in the structure. We stress here that if one would only study N−NH order parameters, one would report this part of the structure as motionally restricted, while the lack of $S^2_{C'-C\alpha}$ order reveals a dynamic behavior. Another case is seen for residue 112, which by N−NH relaxation measurements would be interpreted as ordered, whereas the C′ dynamics indicate that an anisotropic motion exists described as a partial rotation of this peptide plane around the σ_{22} axis, or N−NH bond direction. At the other extreme, where $S^2_{C'-C\alpha}$ is significantly larger than S^2_{N-NH}, anisotropic motion can be modeled with a predominant motion around the σ_{11} axis (see Figure 3a). We find at least 10 residues in flavodoxin that are motionally restricted according to the $S^2_{C'-C\alpha}$ order parameter but which by S^2_{N-NH} order are mobile. Several of these cases are entered in Table 3.

The motional restriction map $S^2_{C'-C\alpha}$ vs S^2_{N-NH} is much less informative in the area close to the diagonal. The diagonal itself indicates many possibilities: correlated isotropic motion or a motional vector anywhere in the plane bisecting the angle between the C′−Cα and N−NH bond vectors. The motional restriction maps $S^2_{C'-C\alpha}$ vs R(CC) and S^2_{N-NH} vs R(CC) can distinguish between many of these cases. Figure 6B shows the comparison of S^2_{N-NH} and C′−Cα/C′−CSA cross-correlation. Here, too, one finds that the experimental data points do not trace out a statistical correlation between these parameters (given by the dashed line). In this case, one could assume that the chemical shift anisotropies are different for different residue types and may thus cause the spread in cross-correlations. As an example, Figure 7 shows the spread in cross-correlations in Alanine residues. It is clear that the spread observed in Figure 6B is already represented within the different amino acids and is thus not associated with the identity of the amino acids. Within an amino acid, the spread is also not caused by differences in secondary structure, since the α-helical residues Ala45 and Ala100 already span most of the spread in cross-correlation rates (Figure 7). As explained in the results section, variation in transverse cross-correlation rates, as we observe here, cannot be caused by flips of the Cα spins provided that these flips are slower than the scalar coupling. Such flips manifest themselves only as an equal lifetime broadening on the two signals as in Figure 5, and thus do not enter into the observed cross-correlation rates which we derive from the ratio of the two peaks. Technical imperfections, such as small excitations of the Cα spins by the π pulse on the C′ spins (see Figure 4), will also affect both C′ doublet components equally, and will not change their ratio.

We therefore propose here, as above, that anisotropic local motion is the major cause of the spread of the cross-correlation rates. This is the most conservative interpretation, because we already propose a model of motional anisotropy in order to understand the lack of correlation between $S^2_{C'-C\alpha}$ and S^2_{N-NH} in Figure 6A. We show in Figures 3C and 6C, in which $S^2_{C'-C\alpha}$ and the cross-correlation rate are plotted against each other, that motional anisotropy can generate a cross-correlation rate span of at least 2 Hz associated with $S^2_{C'-C\alpha}$ order parameters of 0.8 or less. Such a spread is consistent with the experimental data. Not at all consistent with the experimental data is the average value for the calculated cross-correlation. Strongly affecting this average is the location of the point corresponding to $S^2_{C'-C\alpha} = 1.0$. This value is independent of our motional modeling, as it is just given by eq 13. In principle this value could easily be different for different amino acids, or location in the structure, even though we do not see such a correlation in our data. At worst the cross-correlation rates could be determined by all variables, and be uninterpretable. However, in a Florida State University doctoral thesis study by Mr. Teng, working in Dr. Cross' solid-state NMR laboratory, the C′ chemical shift tensors for several amino acid residues in peptides are reported[31] (Table 2). As the table shows, there is hardly any variation among the different residues. Also included in this table are the C′ shift tensors as determined by Oas et al.,[45] which are close to those measured by Teng.[31] We are thus confident that the spread in data is not caused by amino acid type, in accordance with Figure 7. We are aware of many more solid-state NMR studies reporting measurements of the C′ CSA tensor values in amino acids and small peptides. The requirement that we also need the orientation of the tensor axes (eq 13) culls many of the older studies of single-labeled powder samples (only principal values) and leaves us with the relatively few single-crystal or C−N double-labeled powder studies. Further, we judged that the studies of the carboxyl tensors of zwitterionic amino acids are also less relevant for our purposes. That leaves us, to our best knowledge, with just three relevant studies: the work of Oas et al.,[39] in which the Gly tensor is determined for five different tripeptides with a central Gly residue, the thesis of Teng,[31] and the work of Teng et al. on cyclic peptides.[46−48]

An average over the tensors in Table 2 was used to calculate the motional model indicated with the lower lines in Figure 6C. This model is off considerably in location, but not in spread, as discussed above. The second set of lines in Figure 6C is calculated with the tensor for C′ of valine in a cyclic peptide[46] (see Table 2). This set of lines does fit the data considerably better and shows that motional modeling with a realistic tensor can explain the experimental data fairly well. However, we would prefer to rely on the consensus tensor for the C′ chemical shift for our data interpretation. We currently do not have a good explanation for the discrepancy between the model based on that tensor and the data points. However, in Figure 7 we have shifted the theoretical curves based on the average chemical

(45) Oas, T. G.; Hartzell, C. J.; McMahon, T. J.; Drobny, G. P.; Dahlquist, F. W. *J. Am. Chem. Soc.* **1987**, *109*, 5956−5962.
(46) Teng, Q.; Iqbal, M.; Cross, T. A. *J. Am. Chem. Soc.* **1992**, *114*, 5312−5321.
(47) Manuscript in preparation.
(48) Palmer, A. G.; Cavanagh, J.; Wright, P. E.; Rance, M. *J. Magn. Reson.* **1991**, *93*, 151−170. Kay, L. E.; Keifer, P.; Saarinen, T. *J. Am. Chem. Soc.* **1992**, *85*, 393−399.

Table 2. Carbonyl Chemical Shift Anisotropy in Peptides[a]

reference	compound		C′ tensor σ_{11}	σ_{22}	σ_{33}	σ_{iso}	σ_{11*}	σ_{22*}	σ_{33*}	α
Teng[31]	gramicidin Val-Gly	Val	246	169	93	169.3	76.7	−0.33	−76.3	−37
	gramicidin Gly-Ala	Gly	246	162	92	166.7	79.3	−4.67	−74.7	−34
	gramicidin Ala-Leu	Ala	248	170	92	170	78	0	−78	−37
	gramicidin Leu-Ala	Leu	248	170	92	170	78	0	−78	−35
	gramicidin Ala-Val	Ala	247	170	94	170.3	76.7	−0.33	−76.3	−35
Teng et al.[46]	gramicidin	Ala	244	178	90	170.7	73.3	7.333	−80.7	−38
	cyclyc peptide	Val	236	185	105	175.3	60.7	9.667	−70.3	−34
Oas et al.[45]	Ac-Gly-Ala-NH2	Gly	114	56.4	−39	43.83	69.8	12.57	−82.3	−36.6
	Ac-Gly-Gly-NH2	Gly	115	55.7	−37	44.3	70.2	11.4	−81.6	−34.5
	average values						75.2	3.246	−78.5	−35.9

[a] The values σ_{11}, σ_{22}, and σ_{33} are the measured tensor components with respect to the chosen reference compounds; the values σ_{11*}, σ_{22*}, and σ_{33*} give the anisotropy. The average values did not include the values for valine. The angle α is between σ_{11} and the C−N bond vector (see Figure 1).

Table 3[a]

residue	NH order	C′−Cα order	rotational axis NH/C−Cα order	CC rate (−Hz)	rotational axis NH order/CC	consensus
extremes						
14	1.01 ± 0.02	0.81 ± 0.05	22	1.6 ± 0.1	no additional information (a)	22
43	1.00 ± 0.02	0.82 ± 0.04	22	2.2 ± 0.2	no additional information	22
105	0.91 ± 0.02	0.72 ± 0.03	22	2.2 ± 0.2	no additional information	22
112	0.98 ± 0.04	0.67 ± 0.04	22	2.2 ± 0.2	no additional information	22
153	1.09 ± 0.08	0.88 ± 0.03	22	2.4 ± 0.2	no additional information	22
157	0.92 ± 0.04	0.74 ± 0.03	22	2.8 ± 0.2	no additional information	22
158	0.90 ± 0.06	0.67 ± 0.04	22	1.8 ± 0.1	no additional information	22
160	0.95 ± 0.04	0.72 ± 0.03	22	1.8 ± 0.1	no additional information	22
167	0.96 ± 0.04	0.75 ± 0.03	22	2.6 ± 0.2	no additional information	22
1	0.63 ± 0.02	0.96 ± 0.05	11	1.8 ± 0.1	uninterpreted (c)	11
30	0.319 ± 0.009	0.79 ± 0.03	11	3.0 ± 0.2	11 (d)	11
33	0.564 ± 0.009	0.87 ± 0.07	11	2.2 ± 0.1	uninterpreted (b)	11
37	0.78 ± 0.01	1.02 ± 0.04	11	2.1 ± 0.1	uninterpreted (b)	11
45	0.71 ± 0.02	0.88 ± 0.04	11	1.9 ± 0.1	uninterpreted (b)	11
68	0.47 ± 0.01	0.84 ± 0.04	11	2.4 ± 0.2	uninterpreted (b)	11
82	0.71 ± 0.02	0.87 ± 0.04	11	2.6 ± 0.2	uninterpreted (b)	11
113	0.660 ± 0.007	0.88 ± 0.06	11	none	uninterpreted (b)	11
149	0.69 ± 0.02	0.88 ± 0.04	11	2.2 ± 0.1	uninterpreted (b)	11
161	0.25 ± 0.01	0.72 ± 0.02	11	1.8 ± 0.1	uninterpreted (b)	11
pseudocorrelated						
42	0.86 ± 0.02	0.73 ± 0.04	11−22 or 11−33	1.4 ± 0.1	22	close to 22
50	0.70 ± 0.03	0.70 ± 0.05	11−22 or 33	3.1 ± 0.2	11 or 33	33
78	0.73 ± 0.02	0.63 ± 0.04	11−22 or 11−33	0.6 ± 0.04	between 11 and 22	between 11 and 22
90	0.85 ± 0.03	0.71 ± 0.04	11−22 or 33	3.3 ± 0.2	11 or 33	between 11 and 33
115	0.72 ± 0.01	0.72 ± 0.03	11−22 or 33	3.2 ± 0.2	11 or 33	33
134	0.71 ± 0.02	0.62 ± 0.05	11−22 or 33	3.6 ± 0.2	11 or 33	33
alanyl						
Ala 30	0.319 ± 0.009	0.79 ± 0.03	11	3.0 ± 0.2	11	11
Ala 36	0.83 ± 0.03	0.77 ± 0.04	11−22 or 33	1.8 ± 0.01	close to 22	close to 22
Ala 45	0.72 ± 0.02	0.88 ± 0.04	11−22 or 33	1.9 ± 0.1	between 11 and 22	between 11 and 22
Ala 83	0.70 ± 0.03	0.86 ± 0.06	close to 11	2.9 ± 0.2	11 or 33	11
Ala 94	0.76 ± 0.03	0.76 ± 0.03	11−22 or 33	2.3 ± 0.2	33	33
Ala 100	0.85 ± 0.01	0.82 ± 0.05	11−22 or 33	2.8 ± 0.2	33	33
Ala 122	0.71 ± 0.02	0.62 ± 0.07	11−22 or 33	1.8 ± 0.1	between 11 and 22	between 11 and 22
Ala 128	0.68 ± 0.01	0.83 ± 0.03	toward 11	3.1 ± 0.2	11	11
Ala 142	0.88 ± 0.05	0.63 ± 0.04	toward 22	1.9 ± 0.1	between 11 and 22	between 11 and 22
Ala 153	1.09 ± 0.08	0.88 ± 0.03	22	2.4 ± 0.2	no added infor	22

[a] Motional models for several peptide planes of *E. coli* flavodoxin. The Cα residue number was assigned to all of the nuclei of the peptide plane CO−N−NH following that Cα. Column 4 gives the axis of anisotropic rotation as deduced from the order parameters in the columns 2 and 3. Column 6 gives the axis of anisotropic rotation as deduced from the order parameter in columns 2 and the cross-correlation rate in column 5 (in Hz). Column 7 gives the axis of anisotropic rotation consistent with both columns 4 and 6. Residues under the header "extremes" have very different N−NH and C′−Cα order parameters; the data was interpreted using Figure 6A. Residues under the header "pseudocorrelated" have similar order parameters resembling statistical correlation but have cross-correlation rates of extreme values; the data was interpreted using Figure 8. The data for the alanyl residues was interpreted from Figures 6A and 7. Notes: (a) The cross-correlation rates for large N−NH order parameters do not yield extra information (see Figure 6b). (b) The cross-correlation rate is an average value and cannot be interpreted, except for (c) where for the charged Ala 1 a very different C′ CSA may apply and for (d) where a maximum cross-correlation rate for alanyl residues is observed (see also under Ala 30).

shift tensor upward by 1 Hz to better accommodate the experimental data. As will be demonstrated below, this allows for a self-consistent interpretation of S^2_{N-NH}, $S^2_{C'-C\alpha}$, and R(CC).

It is clear that the cross-correlations at $S^2_{C'-C\alpha}$ order parameters close to 1 will be most strongly influenced by any differences in tensor values. Here, we will assume that there is a constant offset in cross-correlation rates and attempt to interpret the data in Figure 6B for those residues that have a $S^2_{C'-C\alpha}$ smaller than 0.8. We have taken only those residues

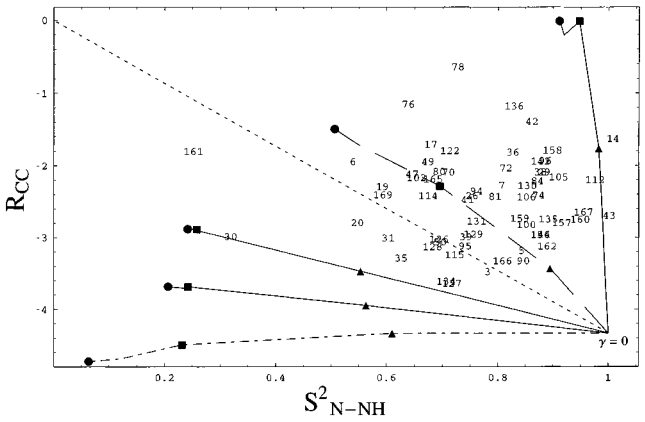

Figure 8. Experimental data for those residues with $S^2_{C'-C\alpha} < 0.8$ showing the C′(CSA)/C′−Cα(dipolar) cross-correlation rate and the order parameter S^2_{N-NH}. Motional models and motional extents are as in Figure 3B.

that have a $S^2_{C'-C\alpha}$ smaller than 0.8 from Figure 6B and plotted them in Figure 8. We will only consider limiting cases. Residues that have a cross-correlation of −3 Hz or more negative must have a motion with a considerable σ_{11} or σ_{33} component. This very conservative analysis yields interesting information for residues 50, 90, 115, and 134 as shown in Table 3. For instance, residue 50 lies on the diagonal in Figure 6A, which indicates a motion about any axis in the plane bisecting the N−NH and C′−Cα bond vectors. Figure 8 shows conclusively that the motional axis must lie perpendicular to the peptide plane (σ_{33}). Residues with very small cross-correlation rates are, e.g., 6, 42, 78, and 136 and are defined as having no large σ_{33} or σ_{11} component in the orientation of their dominant rotational axis. This solves the ambivalence for residues 78 and 42 which are close to the diagonal in Figure 6A. Their rotational axis must lie in the peptide plane, close to the in-plane vector.

We can also cautiously interpret the data for individual amino acids. Assuming that the observed spread of cross-correlation rates is representative for the possible spread, we can "renormalize" our motional restriction maps and use them, on a residue-to-residue basis to distinguish between different motional models. Examples of this analysis are outlined in Table 3 for Ala (Figure 7). It is reassuring to see that possible motional models deduced from the S^2_{N-NH} and $S^2_{C'-C\alpha}$ order parameters can always be fitted with a model deduced from S^2_{N-NH} and the cross-correlation rate. For instance, large cross-correlation rates correspond to large $S^2_{C'-C\alpha}$ parameters and vice-versa, except for Ala 1, where a small cross-correlation rate (−1.8 Hz) is found with a $S^2_{C'-C\alpha}$ parameter of 0.96. A possible explanation for this discrepancy is that the CSA for an N-terminal, charged, residue may be quite different from the average. The combined interpretation of several motional restriction maps results in the characterization of the dynamics of a fair number of residues in flavodoxin. It is interesting to realize that peptide planes, for which the S^2_{N-NH} and $S^2_{C'-C\alpha}$ order parameters are the same and are thus indicating nothing out of the ordinary in Figure 6A, is actually found to have an anisotropic motion along the σ_{33} axis. The peptide plane following residue 50 is a perfect example of this.

In conclusion, we have shown here that it is important to measure relaxation parameters of several vectors in a motional unit, such as a peptide plane, in order to describe its dynamic properties. Studying only one relaxation vector may result in a serious underestimation of the dynamical nature of the protein. Such underestimation will interfere with the correct interpretation of protein backbone dynamics in terms of entropy, or, when ligand binding is involved, with the interpretation of the change in entropy. Here, we use three dynamical parameters: $S^2_{C'-C\alpha}$, S^2_{N-NH}, and the cross-correlation between the C′−Cα and C′−chemical shift anisotropy relaxation in order to better define the peptide plane dynamics. We explicitly reject the notion that local or semilocal peptide−plane dynamics is isotropic, in which case a single order parameter for all its relaxation vectors would apply. In order to interpret the data in terms of anisotropic local or semilocal motion, we have made a modest extension on relaxation theory by combining the work of (mainly) Goldman[34] and Daragan and Mayo.[36] We adopt Daragan and Mayo's motional modeling,[36] as restricted rotations around certain axes, as a good description of the consequences of anisotropic motion in a module that is geometrically linked, such as the vectors C′(*i*)−Cα(*i*), C′(*i*)−CSA, C′(*i*)−N(*i*+1), N(*i*+1)−H(*i*+1), and N(*i*+1)−Cα(*i*+1) in the peptide plane. The results of this study are encouraging. We are able characterize the local dynamics of some 32 residues in the 20 kDa protein flavodoxin of *E. coli*. These peptide−plane studies can be extended by measuring more relaxation data, such as additional cross-correlations and/or single vector dynamics. This should result in better definition of the motional models. The concept of measuring more than one relaxation parameter should also be of importance for the characterization of side-chain dynamics. All our current experiments and theory can be directly transferred to the study of the Asn and Gln amide moieties.

Acknowledgment. This work was supported by grants MCB 9513355 from the National Science Foundation and R01-GM 52406 from the National Institutes of Health. We thank Drs. D. Hoover and M. L. Ludwig for the sample and coordinates for *E. coli* flavodoxin, and Dr. G. Otting for communicating the NMR assignments of flavodoxin to us before publication. We thank Drs. S. Krimm and T. Cross for helpful discussions.

Supporting Information Available: Three figures showing the order parameters $S^2_{C'-C\alpha}$ and S^2_{N-NH} and the cross-correlation between the C′−Cα and C′−chemical shift anisotropy relaxation rate vs residue number for *E. coli* flavodoxin; the figure legends describe the determination of error margins (5 pages). See any current masthead page for ordering and Internet access instructions.

JA972083Y